© 2018. Published by The Company of Biologists Ltd | Development (2018) 145, dev161927. doi:10.1242/dev.161927

RESEARCH ARTICLE

FGF controls epithelial-mesenchymal transitions during gastrulation by regulating cell division and apicobasal polarity

Jingjing Sun and Angelike Stathopoulos*

ABSTRACT

To support tissue and organ development, cells transition between epithelial and mesenchymal states. Here, we have investigated how mesoderm cells change state in *Drosophila* embryos and whether fibroblast growth factor (FGF) signaling plays a role. During gastrulation, presumptive mesoderm cells invaginate, undergo an epithelial-to-mesenchymal state transition (EMT) and migrate upon the ectoderm. Our data show that EMT is a prolonged process in which adherens junctions progressively decrease in number throughout the migration of mesoderm cells. FGF influences adherens junction number and promotes mesoderm cell division, which we propose decreases cell-cell attachments to support slow EMT while retaining collective cell movement. We also found that, at the completion of migration, cells form a monolayer and undergo a reverse mesenchymal-to-epithelial transition (MET). FGF activity leads to accumulation of β-integrin Myospheroid basally and cell polarity factor Bazooka apically within mesoderm cells, thereby reestablishing apicobasal cell polarity in an epithelialized state in which cells express both E-Cadherin and N-Cadherin. In summary, FGF plays a dynamic role in supporting mesoderm cell development to ensure collective mesoderm cell movements, as well as proper differentiation of mesoderm cell types.

KEY WORDS: *Drosophila melanogaster*, Epithelial-to-mesenchymal (EMT), Mesenchymal-to-epithelial (MET), Fibroblast growth factor (FGF), Adherens junction, Integrin, Bazooka

INTRODUCTION

During embryonic development, most tissues arise from a series of cell conversions between epithelial and mesenchymal states (Baum et al., 2008). During epithelial-to-mesenchymal transition (EMT), cells decrease contacts and lose polarity, while the opposite occurs during mesenchymal-to-epithelial transition (MET) as cells regain cell polarity and increase cell-cell adhesion (Thiery et al., 2009). Both processes have been studied because they are pivotal for tissue and organ specification, and also because their misregulation can contribute to metastasis (Nieto, 2013).

In *Drosophila* embryos, the presumptive mesoderm undergoes a series of orchestrated cell movements (Bae et al., 2012; reviewed by Gilmour et al., 2017). Previous studies have focused on the mechanism by which these cells invaginate into the embryos as well as how they initiate migration once internalized. Mesoderm cells express the FGF receptor Heartless (Htl) (Gisselbrecht et al., 1996), whereas the overlying ectoderm expresses the FGF ligands Pyramus (Pyr) and Thisbe (Ths) (Gryzik and Müller, 2004; Stathopoulos et al., 2004). FGF signaling is thought to orient collapse of the invaginated mesodermal tube through chemoattractant-directed movement, whereas signaling is likely not required to support directed migration because a subset of cells moves directionally even in the absence of FGF signaling (McMahon et al., 2008; Muha and Müller, 2013; Murray and Saint, 2007; Wilson et al., 2005). At the end of the spreading process, mesoderm cells form a monolayer; FGF signaling is required to help establish this organization, as the mesoderm remains multilayered in mutants (McMahon et al., 2010). This multilayered phenotype, specifically, is also exhibited by mutants of the *myospheroid* (*mys*) gene, which encodes β-PS integrin (Leptin et al., 1989; MacKrell et al., 1988). Mys protein is localized at the interface between mesoderm and ectoderm at the end of the spreading process, as the monolayer is formed (Roote and Zusman, 1995). In FGF mutants, Mys expression is predominantly lost from the mesoderm-ectoderm interface (McMahon et al., 2010).

Here, we have investigated whether FGF signaling has additional roles in supporting *Drosophila* mesoderm cell migration that relate to EMT and MET. During gastrulation of vertebrate embryos, FGF supports mesodermal EMT by regulating levels of E-Cadherin transcription (Ciruna and Rossant, 2001); in *Drosophila,* this process is thought to be FGF independent, as collapse of the invaginated tube (considered the fly equivalent EMT) does occur in FGF mutants, albeit misdirected. However, in a recent study, we determined that the *htl* gene is maternally provided (Irizarry and Stathopoulos, 2015), opening up the possibility that the zygotic mutants characterized in previous studies exhibit only partial loss-of-function phenotypes. Furthermore, as the mutants fail to specify a mesoderm monolayer at the end of the spreading process at gastrulation (McMahon et al., 2010), we also assayed whether the FGF signaling pathway is involved in re-establishing cell polarity within mesoderm cells in order to support their subsequent differentiation into different cell lineages.

RESULTS

To provide insight into the role of FGF signaling in supporting mesoderm cell migration during *Drosophila* gastrulation, we examined the localization of the FGF receptor Htl. Antibody staining of endogenous protein or Htl-mCherry fusion protein (Irizarry and Stathopoulos, 2015) shows localization at the apical side of cells within the invaginated mesodermal tube (Fig. 1A,D″,D‴, E″,E‴, Fig. S1A,D-F). At collapse, when mesoderm cells begin their migration, Htl becomes enriched at the side of cells in contact with the ectoderm, especially within protrusions that invade the ectoderm (Fig. 1B,E″,E‴,G″,G‴, Fig. S1B,F,H), and remains enriched at the mesoderm-ectoderm boundary even when a monolayer forms (Fig. 1C,H″,H‴, Fig. S1C,I). This localization pattern suggests that FGF signaling may be involved in regulating cell-cell contacts, possibly through modification of adherens junctions (AJs).

California Institute of Technology, Division of Biology and Biological Engineering, 1200 East California Boulevard, Pasadena, CA 91125, USA.

*Author for correspondence (angelike@caltech.edu)

A.S., 0000-0001-6597-2036

Received 29 November 2017; Accepted 31 August 2018

Development (2018) 145, dev161927. doi:10.1242/dev.161927

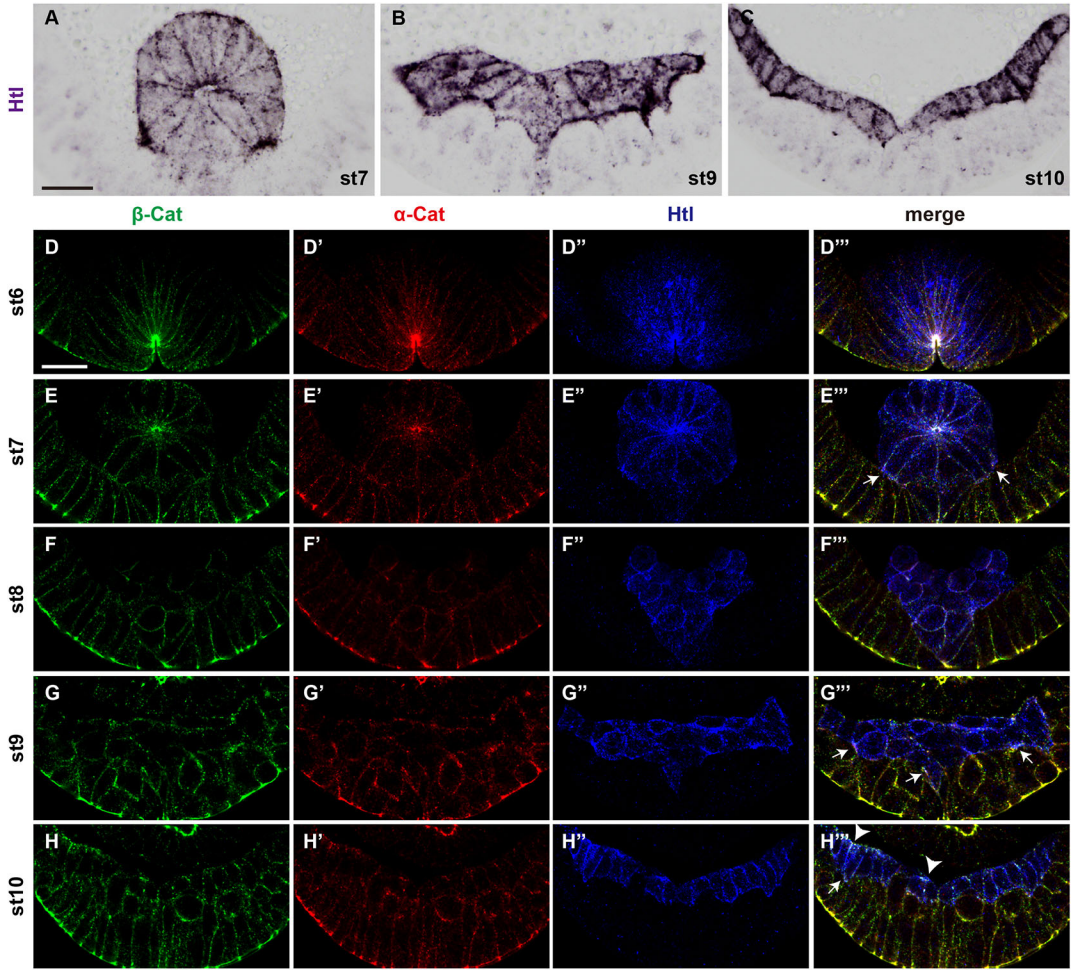

Fig. 1. Dynamic expression pattern of the FGF receptor Htl in the mesoderm during gastrulation and localization of adherens junctions. (A-C) Immunostaining of endogenous Htl expression at the indicated stages using an anti-Htl antibody (Michelson et al., 1998). (D-H‴) Individual and colocalized staining of β-Catenin (β-Cat, green), α-Catenin (α-Cat, red) and Htl (blue) by immunofluorescence in cross-sections of embryos at the indicated stages. Colocalization of all three proteins displays as white signal. Arrows and arrowheads indicate colocalization at the mesoderm-ectoderm or mesoderm-yolk interfaces, respectively. Scale bars: 20 µm.

We detected adherens junctions present in mesoderm cells over the course of migration using the colocalization of α- and β-Catenin, two proteins associated with AJs (Fig. 1D-H,D′-H′) (Baum and Georgiou, 2011; Oda et al., 1998; Tepass et al., 2001). AJs are concentrated at the apical side of invaginated mesoderm cells early on (Kolsch et al., 2007; Weng and Wieschaus, 2016), and we found that Htl is also concentrated in the same position (Fig. 1D‴). As the tube collapses, AJs become newly concentrated at the positions in which the mesoderm contacts the ectoderm (Fig. 1E‴, arrows) as do Htl and E-Cadherin (Fig. S1D-F). Later, immediately before cells divide, only diffuse staining of α- and β-Catenin is present, suggesting contact of rounded mesoderm cells with the ectoderm is weakened (Fig. 1F-F‴, Fig. S1G). As the mesoderm cells initiate their dorsally directed spreading movement, AJs are detectable again and enriched at the mesoderm-ectoderm interface, together with Htl (Fig. 1G‴, arrows) and E-Cadherin (Fig. S1H). At the end of the mesoderm-spreading process, when cells establish a monolayer organization, AJs are found at both mesoderm-ectoderm and mesoderm-yolk interfaces (Fig. 1H‴, arrow and arrowheads, respectively) as described previously by electron microscopy studies (Tepass and Hartenstein, 1994).

To investigate a role for FGF in regulating AJs, the number of AJs was counted within the mesoderm in control embryos as well as in various FGF mutant backgrounds from stage 7 to 10 using colocalization of α- and β-Catenin as a proxy (Fig. 2D,D′; and see Materials and Methods). To start, AJ number in htl^{AB42} zygotic mutant (htl^{M+Z-}; Gisselbrecht et al., 1996) embryos was compared with control (htl^{AB42}/+ heterozygotes, which exhibit normal mesoderm spreading) (Fig. 2A,B). No difference between samples was identified at stages 7 and 8 (Fig. 2E). However, htl^{M+Z-} embryos had significantly fewer AJs at the end of the mesoderm-spreading process (stage 9/10) compared with control (Fig. 2E, orange line-associated asterisk, $P<0.05$), demonstrating a role for zygotic Htl in supporting increased AJ number during monolayer formation, which occurs at stage 9/10. To analyze a maternal role for Htl, we isolated embryos from females containing germline clones of the htl^{AB42} loss-of-function mutation (i.e. htl^{M-Z-}) (Irizarry and Stathopoulos, 2015). In htl^{M-Z-} embryos, AJs were more abundant at stage 7 but also failed to increase at stage 9/10, when compared with control (Fig. 2E, gray line-associated asterisks, $P<0.05$); in embryos from germline clones that were zygotically rescued (htl^{M-Z+}), AJ numbers were similar to control at all stages (Fig. 2E).

These results show that either maternal or zygotic *htl* expression is sufficient to support normal number of AJs at stage 7, whereas zygotic, but not maternal, *htl* expression is required at stage 9/10 to support an FGF-dependent increase in AJ number. This analysis

Development (2018) 145, dev161927. doi:10.1242/dev.161927

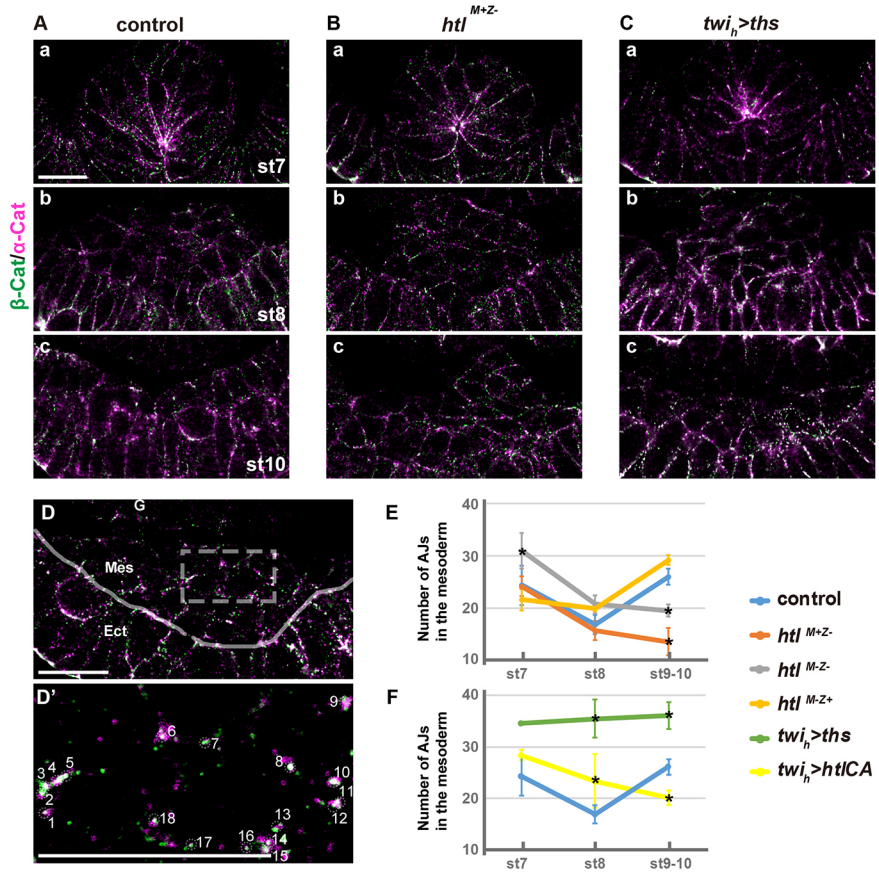

Fig. 2. Quantification of AJ dynamics through α-Catenin and β-Catenin colocalization in the mesoderm at different stages of gastrulation. (A-C) Examples of *z*-projections from confocal scans of stage 7-10 embryos co-stained by antibodies against α-Catenin (violet) and β-Catenin (green) from control (A), htl^{M+Z-} (B) and twi_h>*ths* (C) mutants. (D,D′) An example of how colocalized α-Catenin and β-Catenin are used to infer AJ number. A magnified view of the area outlined in D is shown in D′. White puncta represent colocalized α-Catenin and β-Catenin scored to infer AJ number. In D, the mesoderm-ectoderm boundary is marked by a transparent line to show how AJs were scored only in the mesoderm area. Mes, mesoderm; Ect, ectoderm; G, gut. (E,F) Number of AJs in the mesoderm from stage 7 to 10 in the indicated genetic backgrounds. Control refers to a heterozygous zygotic *htl* mutant (i.e. htl^{M+Z-}/+). Error bars represent s.d. (**P*<0.05, Student's *t*-test). Numbers of embryos for each genetic background at stages 7, 8 and 9-10, respectively, are as follows (total number of z-projections counted in the group is indicated in parentheses): control, 5(43), 5(51) and 3(24); htl^{M+Z-}, 3(25), 7(70) and 6(53); htl^{M-Z-}: 6(60), 4(40) and 4(41); htl^{M-Z+}, 4(39), 3(27) and 3(27); twi_h>*ths*, 1(8), 4(32) and 3(25); twi_h>*htlCA*, 2(21), 3(25) and 3(24). Scale bars: 20 µm.

defines a role for Htl in regulating AJ number at gastrulation, the earliest characterized role for maternal Htl in the embryo, and suggests that FGF has distinct roles in the mesoderm at different stages. The observed decrease in AJ number from stage 7 to stage 8 supports the view that mesoderm cells exhibit a prolonged EMT process, as suggested by previous studies (e.g. Schafer et al., 2014), whereas the increase in AJ number measured at later stages 9/10 likely relates to a previously unappreciated process during mesoderm development.

To provide further insight into the role of FGF signaling, gain-of-function mutants were investigated. The FGF ligand Ths or constitutively active FGF receptor Htl (HtlCA) was ectopically expressed within the mesoderm cells at high levels using the twist-Gal4 driver (twi_h-Gal4; Carmena et al., 1998; Greig and Akam, 1993). Previous studies have shown that, in both cases, mesoderm spreading is aberrant, multilayered and uneven (Kadam et al., 2009). We found that ectopic expression of Ths ligand resulted in consistently high AJ number (Fig. 2C,F; green line-associated asterisks, P<0.05), whereas constitutively active receptor had a smaller, though reproducible, effect in which AJ numbers were increased at earlier stages but decreased at later stage 9/10 relative to the control (Fig. 2F; yellow line-associated asterisks, P<0.05). We hypothesized that both levels as well as direction of FGF receptor activation are important, as these variables have been shown to impact FGF function in other systems (e.g. Cota and Davidson, 2015).

FGF signaling regulates cell polarity once a monolayer is specified

To further understand the changes in AJs during mesoderm development, we investigated the localization of the cell polarity protein Bazooka (Baz), which has been found to act upstream of AJs in the establishment of epithelial polarity (Harris and Peifer, 2004; Laprise and Tepass, 2011). Baz protein is apically localized in the epithelialized *Drosophila* early embryo (Fig. 3A, stages 6-10) as well as within neuroblasts (NB), which are large cells present between the mesoderm and ectoderm (Fig. 3A, stages 9 and stages 10; Fig. 3E) (Roegiers et al., 2001). Recent studies have shown that Baz becomes concentrated at the apical side of cells within the invaginated mesodermal tube (Fig. 3A, stage 7) and is subsequently lost following tube collapse (Weng and Wieschaus, 2017). Nevertheless, we found that some Baz staining remains in puncta at cell-cell contacts throughout the mesoderm-spreading process, which likely correspond to AJs because α- and β-Catenin also colocalize (Fig. 3A, stage 8 and stage 9; data not shown). At the end of mesoderm migration, cells form a monolayer, and, surprisingly, Baz was found to localize to the side of mesoderm cells facing the yolk (Fig. 3A, stage 10).

Baz localization in FGF mutants is aberrant. In htl^{M+Z-} mutants, Baz protein remains clustered after tube collapse, whereas in control embryos, expression is scattered throughout the mesoderm (Fig. 3G, G′ compare with 3F,F′). At stage 10, Baz exhibits only partial localization to the presumptive apical side of mesoderm cells in the absence of zygotic Htl (Figs 3I,I′ and 4A,B, asterisk, P<0.0001) compared with clear localization to the presumptive apical side of mesoderm cells in the control (Fig. 3H,H′). Baz expression is even more noticeably reduced in the mesoderm of htl^{M-Z-} mutants at stage 10 (Fig. 3J,J′ compare with H,H′, Fig. 4B), although expression is detectable at earlier stages in scattered positions between cells as in the zygotic mutant (data not shown). Similar results were also obtained when embryos were analyzed by

Development (2018) 145, dev161927. doi:10.1242/dev.161927

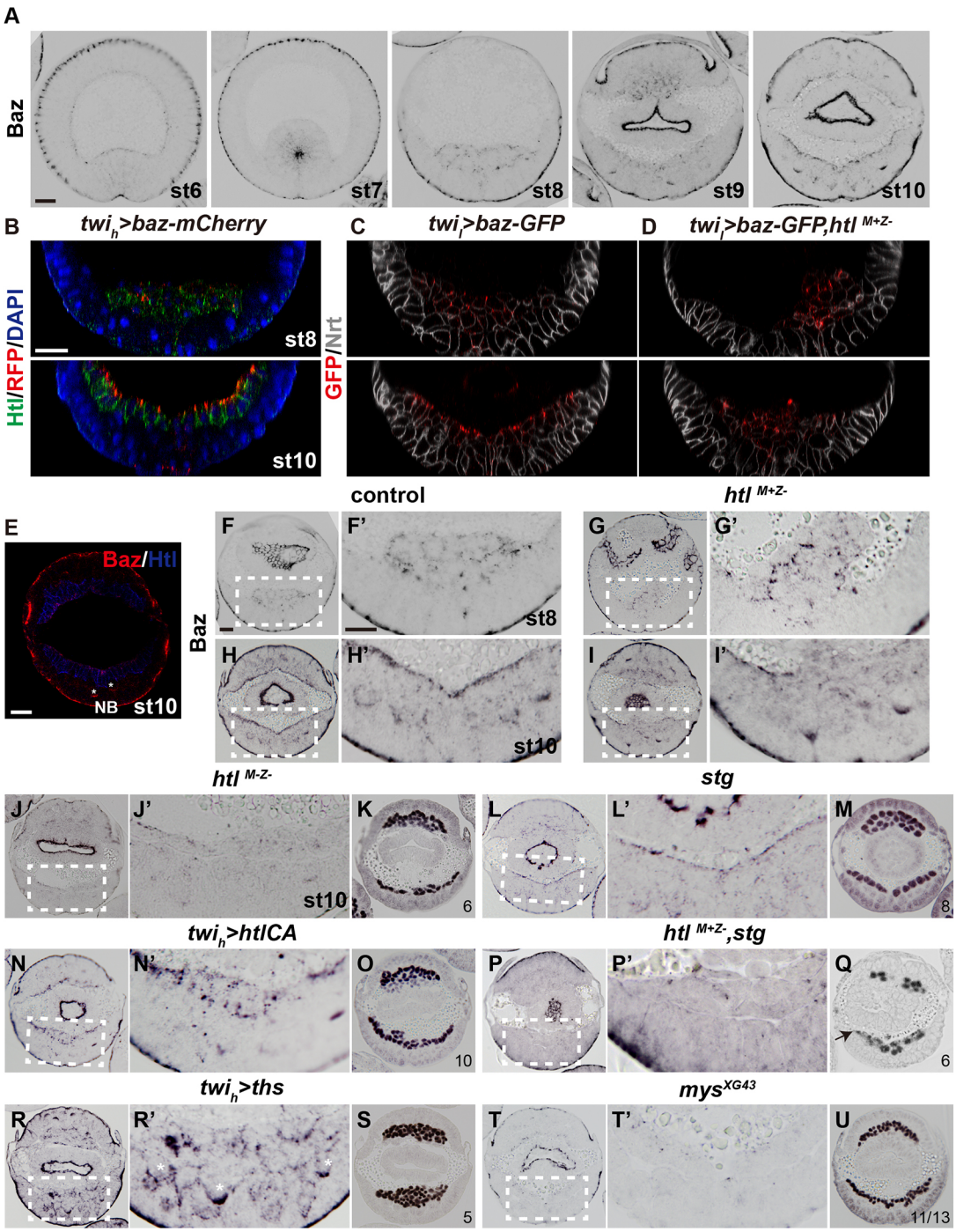

Fig. 3. FGF signaling directs the localization of the polarity protein Baz in the mesoderm cells at the yolk interface. Cross-section of embryos at indicated stages. (A) Baz localization from stage (st) 6 to 10 determined by anti-Baz immunostaining. (B-D) *Z*-projections from confocal scans taken from embryos expressing *baz-mCherry* (B) or *baz-GFP* (C,D) fusion proteins stained using anti-RFP (red, B) or anti-GFP (red, C and D) to detect Baz localization. *baz-mCherry*-expressing embryos were also stained using anti-Htl antibody (green, B) and DAPI (blue, B). *baz-GFP*-expressing embryos were also co-stained using anti-Neurotactin (Nrt; light gray, C and D) to visualize cell outlines, and Baz localization compared in control (C) and *htl* zygotic mutant background (D). (E) Colocalization of Baz (red) and Htl (blue) proteins in an embryo at stage 10 using antibody staining. In addition to its localization at the sub-apical junction complex within the ectoderm, Baz is also localized to the mesoderm-yolk interface, as well as to delaminating neuroblasts. Neuroblasts (NBs) are indicated by asterisks. (F-U) Baz localization in the mesoderm identified by immunostaining with anti-Baz antibody in control (F,F′,H,H′), in *htl* zygotic mutant (G,G′,I,I′), in embryos derived from *htl* germline clones (J,J′) and in *string* (*stg*) mutants (L,L′). High level ectopic expression of constitutively active Htl (HtlCA) in the mesoderm (N,N′) and in the htl^{M+Z-},*stg* double mutant (P,P′). Ectopic expression of *ths* in the mesoderm (R,R′) and *mys* germline clone embryos (T,T′). Boxed regions in F-T are shown at higher magnification in F′-T′. (K,M) Twist localization in embryos derived from *htl* germline clones (K) and in a *stg* mutant (M). (O,Q) High level expression of HtlCA in mesoderm (O) and in a htl^{M+Z-},*stg* double mutant (Q). (S,U) Ectopic *ths* expression in the mesoderm (S) and in mys germline clones (U). Arrow in Q indicates the region of monolayer formation in the htl^{M+Z-},*stg* mutant. Despite the ability of the mesoderm to sometimes form a monolayer in the htl^{M+Z-},*stg* mutant embryo (arrow, Q), Baz expression is never observed in this background (P,P′). Asterisks in R′ indicate neuroblasts. mys^{XG43} refers to *M*−*Z*−. Number of embryos analyzed by Twi antibody staining at stage 10 is indicated in the bottom right-hand corner in K,M,O,Q,S,U. Eleven out of 13 mys^{XG43} germline clone embryos exhibit a non-monolayer phenotype (U). Control refers to a heterozygous zygotic *htl* mutant (i.e. htl^{M+Z-}/+). Scale bars: 20 µm.

Development (2018) 145, dev161927. doi:10.1242/dev.161927

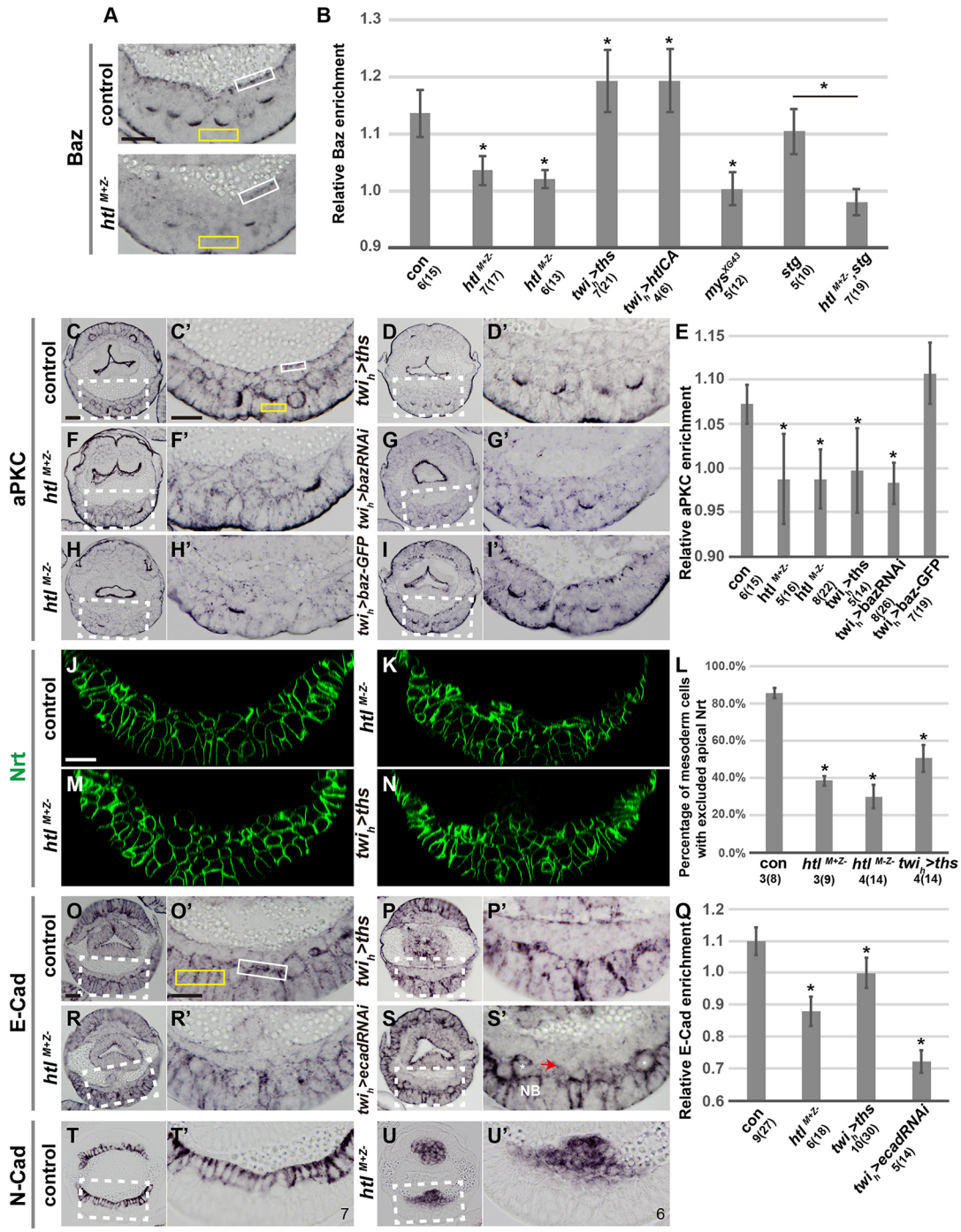

Fig. 4. Mis-localization of aPKC, Neurotactin, E-Cad and N-Cad in the mutants further supports a role for FGF signaling in establishing polarity in the mesoderm. Stage 10 control and mutant embryos are depicted. Boxed regions are shown as magnified views in the panels on the right. Number of embryos and sections (inside the parentheses) are indicated underneath the genotype in the charts. (A,B) Quantification of relative Baz enrichment in the mesoderm in Fig. 3H′, I′,J′,L′,N′,R′,T′. Example of ROI selection in the mesoderm and the ectoderm are indicated by the white and yellow boxes, respectively, in A. *P<0.05. (C,C′) aPKC is localized to the yolk-mesoderm interface similar to Baz, at the presumptive apical side of cells once they form a monolayer. (D,D′,F,F′,H,H′) Loss of function in *htl* (F,F′,H,H′) or ectopic expression of the ligand *ths* within the mesoderm (D,D′) disrupts this localization. (G,G′,I,I′) aPKC expression is dependent on *baz*. (E) Quantification of relative aPKC enrichment in the mesoderm in C′,D′,F′,G′,H′,I′ (*P<0.01). Boxed areas in C′ are examples of selected ROIs. (J-N) *Z*-projections from confocal scans taken from control and mutant embryos stained using anti-Nrt antibody. (J) Nrt is excluded from the apical side of mesoderm cells and concentrated at lateral domains. (K-N) Nrt localization in mutants becomes disorganized. (L) Quantification of the percentage of polarized mesoderm cells in which Nrt is excluded from the apical side in the control and mutant embryo (*P<0.001). (O,O′) At the end of mesoderm spreading, E-Cad accumulates at both the basal side of cells at the mesoderm-ectoderm interface and weakly at apical side of cells at the yolk-mesoderm interface. (P-R′) Both *ths* and *htl* mutants exhibit small decreases in E-Cad at the interface. (Q,S,S′) Knocking down E-Cad in the mesoderm with the *twi$_h$-GAL4* driver significantly reduces expression in both domains but expression in neuroblasts (NB, white asterisks) appears normal as expected. (S′) The red arrow indicates mesoderm-ectoderm interface where E-Cad levels are greatly reduced. (Q) Quantification of relative E-Cad enrichment in O′,P′,R′,S′ (*P<0.001). Examples of selected ROIs are shown in O′. (T-U′) N-Cad accumulates at apical and lateral sides of the epithelialized mesoderm monolayer in the control embryo (T,T′), whereas in *htl* mutants this pattern is disrupted (U,U′). Control refers to a heterozygous zygotic *htl* mutant (i.e. *htl*$^{M+Z-}$/+). Scale bars: 20 µm.

Development (2018) 145, dev161927. doi:10.1242/dev.161927

fluorescence-based staining using the same antibody, or using an anti-RFP or anti-GFP antibody to localize Baz-mCherry or Baz-GFP fusion protein (Fig. 3B-D, Fig. S1J,K,M-T). When co-stained with an anti-Htl antibody, we also discovered that Htl and Baz do not colocalize once a monolayer is specified (Fig. 3B).

To investigate whether FGF indirectly supports cell polarity by acting to support monolayer formation, we analyzed the localization of Baz in a htl^{M+Z-},*stg* double mutant background in which monolayer formation is partially restored (arrow, Fig. 3Q) as opposed to the multi-layered, uneven mesoderm observed in htl^{M+Z-} single mutant embryos (e.g. Fig. 3I). *string* (*stg*) encodes a Cdc25-type phosphatase that regulates cell division (Edgar and O'Farrell, 1989). Normally, mesoderm cells divide twice during gastrulation; these divisions fail to occur in *stg* mutants, resulting in a monolayer with much fewer cells (Fig. 3M) (Leptin and Grunewald, 1990). However, Baz localization is undisrupted (Figs 3L,L′ and 4B). In contrast, Baz localization to the apical side is significantly diminished in htl^{M+Z-},*stg* double mutants (Fig. 3P,P′ compare with L,L′, Fig. 4B), despite the increased propensity of the mesoderm to achieve a monolayer when compared with htl^{M+Z-} single mutants.

Furthermore, expression of FGF ligands or HtlCA in the mesoderm at high levels results in both aberrant migration (Fig. 3O,S; Michelson et al., 1998; Stathopoulos et al., 2004) and mislocalization of Baz (Figs 3N,N′,R,R′ and 4B, Fig. S2C,C′). Collectively, these results support the idea that FGF signaling is important for correct localization of Baz protein.

More generally, these results also suggest that mesenchymal cells transition to an epithelial-like state by regaining cell polarity at stage 9/10 when they form a monolayer. We examined localization of other cell polarity markers, including: atypical protein kinase C (aPKC), which is often located at the apical domain of cells (Wodarz et al., 2000); Myospheroid (Mys), which is often located on the basal side (Fernandes et al., 2014; Narasimha and Brown, 2013); as well as Neurotactin (Nrt), which is excluded from apical domains but present in basolateral regions (Müller and Wieschaus, 1996). Like Baz, aPKC was found to localize to the presumptive apical side of mesoderm cells at stage 9/10 once the monolayer is achieved (Fig. 4C,C′). This localization of aPKC is lost in *htl* mutants (Fig. 4E-F′,H,H′), upon ectopic expression of *ths* ligand in the mesoderm (Fig. 4D-E), or when Baz level is reduced in the mesoderm using tissue-specific RNAi (Fig. 4E,G,G′). Localization of aPKC to the apical domain appears reinforced upon ectopic expression of Baz-GFP in the mesoderm (Fig. 4E,I,I′). Nrt localization was also affected, as it was no longer excluded from the presumptive apical domain of cells in FGF gain or loss of function mutants (Fig. 4J-L). Previous studies had found that FGF signaling is required to support expression of the β-PS1 integrin Mys at the interface between mesoderm and ectoderm cells at the end of mesoderm spreading at stage 9/10 (McMahon et al., 2010). Additionally, through expression of a Mys RNAi line in the mesoderm, we defined that Mys expression in ventral regions is mesodermally derived (Fig. S2G,G′). Even less Mys is present at the mesoderm-ectoderm interface in embryos obtained from females containing htl^{AB42} germline clones (htl^{M-Z-}) (Fig. 5I,I′ compare with 5A,A′ and 5E,E′,Q). This decrease likely relates to an FGF-direct effect on Mys protein, as transcript levels are not substantially changed in the mutant (Fig. S2I,J). Taken together, these data demonstrate that mesoderm cells acquire an apico-basal polarity, in which Baz, aPKC, Nrt and Mys are spatially localized within cells, and that this process is regulated by FGF signaling.

We also investigated the relationship between basally localized Mys and apically localized Baz, which influence the localization of one another in other cell systems (e.g. Fernández-Miñán et al., 2008). In embryos derived from mys^{XG43} germline clone females (mys^{M-Z-}) (Boube et al., 2001; Leptin et al., 1989), which lack Mys expression (Fig. S2K-L,R), Baz expression was either greatly diminished or completely lost (Figs 3T,T′ and 4B). In turn, upon ectopic expression of Mys in the mesoderm, mesoderm cells formed a multilayer organization with only low levels of Baz localized to the apical position in regions where a monolayer is achieved (Fig. S2D-F′). Reducing Baz levels in the mesoderm through RNAi resulted in loss of Mys expression in the ventral region (Fig. S2N-O,R). Therefore, Mys and Baz appear to regulate each other.

To examine whether these mesoderm cells completely switch to an epithelial state and/or retain mesenchymal characteristics, we examined expression of E-Cadherin (E-Cad) and N-Cadherin (N-Cad), cell-adhesion molecules typically associated with either epithelial cells or mesenchymal cells, respectively (Iwai et al., 1997; Oda et al., 1994). Several studies have reported their expression dynamics and reciprocal regulation known as the 'Cadherin switch': as E-Cad levels decrease in the mesoderm, N-Cad levels increase (Oda et al., 1998; Schafer et al., 2014). Surprisingly, we found that E-Cad and N-Cad are co-expressed at the monolayer stage and exhibit spatially biased localization within cells. N-Cad is expressed in the apicolateral domain (Fig. 4T,T′), while E-Cad is present at both the mesoderm-ectoderm interface and the mesoderm-yolk interface at low levels (Fig. 4O,O′). Performing tissue-specific E-Cad RNAi in the mesoderm led to loss of E-Cad from both interfaces (Fig. 4Q,S,S′), indicating that E-Cad expression is indeed mesoderm derived (Clark et al., 2011). Whether expression of E-Cad at the monolayer stage is regained or perdures from earlier stages and becomes differentially localized remains unclear; however, the presence of E-Cad at the monolayer stage further supports the view that mesoderm cells undergo an MET, in which they exhibit characteristics of epithelial cell fate. The 'hybrid Cadherin state' uncovered, in which both E-Cad and N-Cad are co-expressed but differentially distributed within cells, is suggestive of distinct functions for these cadherins (see Discussion).

Ectopic FGF expression results in precocious expression of adhesion molecules before cell polarity is properly established

We hypothesized that local activation of the FGF receptor supports the definition of basal cell polarity by controlling Mys localization as Htl protein re-localizes to the presumptive basal cell surface after tube collapse (see Fig. 1B) and ligands Pyr and Ths are expressed in the overlying ectoderm (Kadam et al., 2009). Low-level expression of the wild-type *htl* cDNA using a different twist-Gal4 driver (twi_l-*GAL4*) (Lee et al., 2003; Marqués et al., 2002) can rescue *htl* zygotic mutant phenotypes to support monolayer formation (six out of seven embryos, Fig. 5H,P) and localized expression of Mys and Baz (Fig. 5G,G′,O,O′,Q,R). Expression of HtlCA in the same manner can also support monolayer formation in a fraction of embryos (five out of eight embryos, Fig. 5D,L) but, in contrast, little rescue of the Mys and Baz phenotype was observed (Fig. 5C,C′ compare with Fig. 5E,E′; Fig. 5K,K′, compare with Fig. 3I,I′; 5Q,R).

In contrast, ectopic expression of either HtlCA or ligands at higher levels in the mesoderm using twi_h-*Gal4* driver resulted in severe multilayered mesoderm phenotypes in which both Mys (Fig. 5M,M′,N,Q, Fig. S2A,A′,B,S,S′,T,R) and Baz, as previously discussed (Figs 3N,N′,R,R′, 4A and Fig. S2C,C′M), are ectopically expressed. Under similar conditions, no ectopic expression was observed for aPKC (Fig. 4D-E), Nrt (Fig. 4N) and E-Cad at the meso-ectoderm interface (Fig. 4P-Q).

Development (2018) 145, dev161927. doi:10.1242/dev.161927

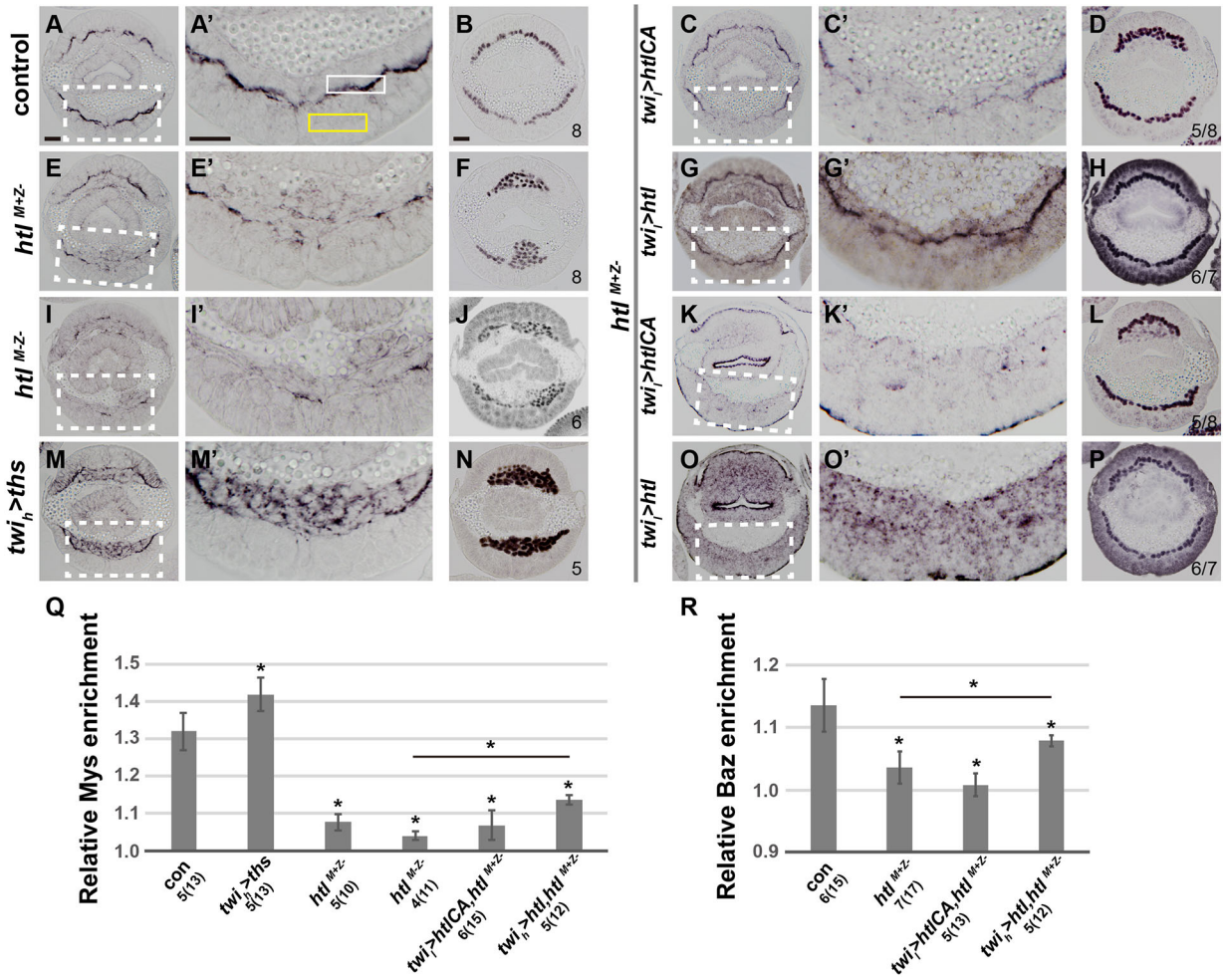

Fig. 5. *htl* functions to support expression of Mys at the mesoderm-ectoderm interface to define basal polarity of mesoderm cells. (A-P) Cross-sections of stage 10 embryos stained using anti-Mys (A,C,E,G,I,M), anti-Baz (K,O) or anti-Twi (B,D,F,H,J,L,N,P) antibodies. For anti-Mys and anti-Baz staining, boxed areas are shown at higher magnification on the right. Genotypes are indicated on the left. The variability in anti-Twi background relates to whether or not the embryos were co-stained with anti-β-gal antibody to identify balancer chromosomes (see Materials and Methods). Number of stage 10 embryos analyzed using Twi antibody staining is indicated in the bottom right-hand corner in B,D,F,H,J,L,N,P. Ratios in D,H,L,P represent the percentages of embryos that were rescued to exhibit a monolayer mesoderm. (Q) Quantification of relative Mys enrichment in A′,E′,G′,I′,M′,O′. Examples of the selected ROIs at the meso-ectoderm interface and the ectoderm are indicated by the white and yellow boxes, respectively, in A′. (R) Quantification of relative Baz enrichment in C′ and K′ compared with the controls and htl^{M+Z-} mutants (see Fig. 4A,B). Number of embryos and sections (inside the parenthesis) are indicated underneath the genotype (*P<0.005). Control refers to a heterozygous zygotic *htl* mutant (i.e. htl^{M+Z-}/+). Scale bars: 20 µm.

Collectively, these results demonstrate that the direction of FGF signaling is important for the acquisition of cell polarity at the end of mesoderm migration at the monolayer stage, whereas levels, but not necessarily direction, of signaling is important for mesoderm EMT (i.e. collapse and spreading). These results also suggest that FGF regulates localization of Baz and Mys to support cell polarity.

Bazooka and Myospheroid levels are important for even distribution of distinct muscle cell types

We reasoned that monolayer formation and/or polarity may influence differentiation of muscle cell types by ensuring even distribution of mesoderm cells upon the ectoderm. FGF signaling supports spreading of the mesoderm, such that cells may contact the dorsal ectoderm and be induced by signaling pathways active there to specify distinct cell types, including visceral mesoderm and pericardial cell/dorsal somatic lineages marked by *bagpipe* (*bap*) and *even-skipped* (*eve*) expression, respectively (e.g. Frasch, 1995; Frasch et al., 1987; Staehling-Hampton et al., 1994). For example, *eve* transcription requires both FGF and Dpp signaling, whereas *bap* expression is supported directly by Dpp signaling but requires FGF signaling only indirectly to support spreading (see Fig. 6B, compare with 6A; e.g. Stathopoulos et al., 2004). We assayed various mutant backgrounds that affect *baz* and *mys* levels, and found that the greater the associated non-monolayer phenotype, the less uniform the expression of *bap* or Eve observed (Fig. 6). For example, tissue-specific RNAi of *baz* or ectopic expression of *mys* supports non-uniform expression of *bap* transcript or Eve protein (arrows and arrowhead, Fig. 6E,G,J,L, also see Fig. S2E,H,N,P for spreading phenotypes), whereas *mys* loss-of-function mutants were less severe (Fig. 6D,F,H). Uniform mesoderm migration and monolayer formation likely ensures that the proper number of mesoderm cells contact ectoderm cells in order that the mesoderm can be induced to form all the various muscle lineages. In addition, the polarized localization of signaling regulators such as Mys to the mesoderm-ectoderm interface may support levels/efficiency of signaling pathway activation (Sawala et al., 2015; see Discussion).

Development (2018) 145, dev161927. doi:10.1242/dev.161927

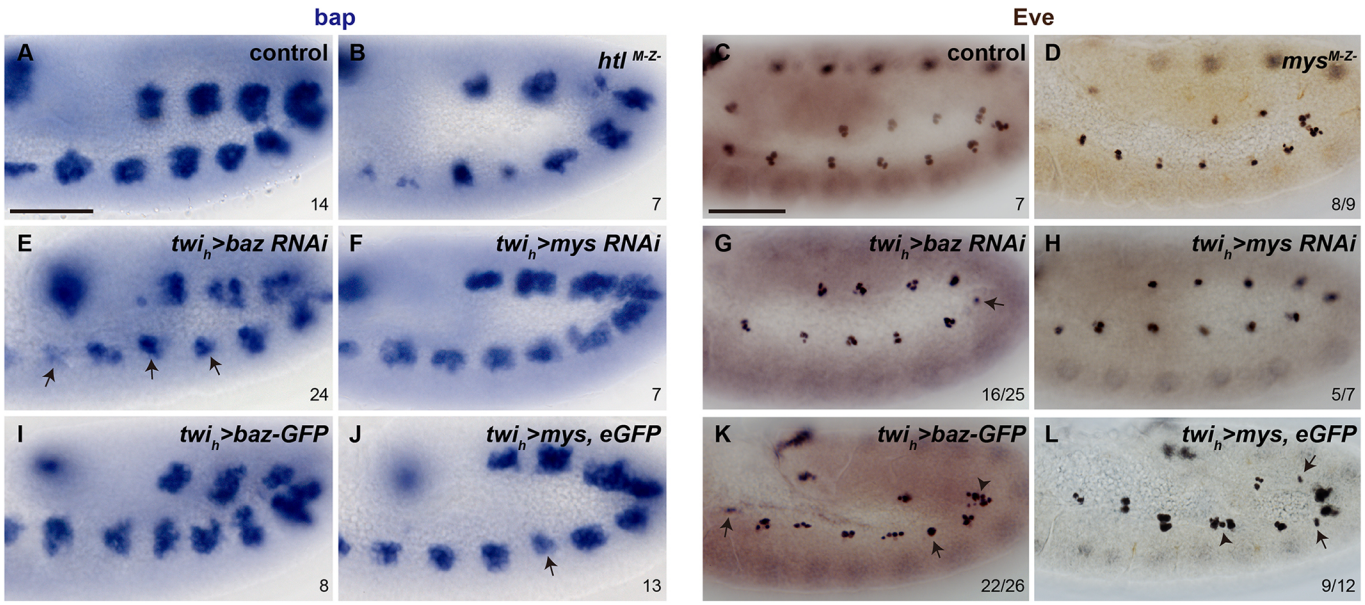

Fig. 6. Changes in *baz* or *mys* levels within the mesoderm result in abnormal distribution of visceral mesoderm and pericardial cells. (A,B,E,F,I,J) *bap* expression was detected by *in situ* hybridization using a riboprobe to mark the visceral mesoderm cells at stage 10 in control embryos (A) or indicated mutant backgrounds (B,E,F,I,J). In the *htl* mutant, the patches of *bap*-positive cells are uneven in size compared with the control, with expression in some hemisegments appearing much smaller/absent (B, compare with A). This phenotype is variable and less severe in the mutants that downregulate or upregulate *baz* or *mys* in the mesoderm (F,I,J), except for twi_h*>baz RNAi*, which seems to cause a comparably strong defect in *bap* expression (arrows, E). (C,D,G,H,K,L) Stage 11 embryos of indicated genotypes were immunostained with an anti-Even-skipped (Eve) antibody to show pericardial cells. In control embryos (*yw*), these cells are arranged in 11 clusters of two to four cells each (C). Misregulation of either *baz* or *mys* leads to abnormal distribution of Eve-positive cells. The more severe the mesoderm defect, the less uniform Eve expression is among the clusters. The twi_h*>baz RNAi*, twi_h*>baz-GFP* and twi_h*>mys,eGFP* embryos shown are missing one or more clusters of pericardial cells, with only one Eve-positive cell in some hemisegments (arrows, G,K,L) and more than four in others (arrowheads, K,L). Number of embryos analyzed is indicated in the bottom right-hand corner. Ratios are given only if phenotype is variable and represent the percentage of embryos with phenotype similar to that shown. Scale bars: 50 µm.

Live *in vivo* imaging and tracking analysis provides novel insight into the collective movement of mesoderm and cell division phenotypes

We hypothesized that the widespread expression of Mys/Baz upon FGF gain-of-function influences the ability of mesoderm cells to migrate properly. Live *in vivo* imaging coupled with tracking analysis was used previously to investigate the htl^{M+Z-} mutant phenotype (McMahon et al., 2008) and the *mys* mutant phenotype (McMahon et al., 2010). An H2A-GFP transgene (Clarkson and Saint, 1999) is used to image mesoderm cell movements in time over the course of mesoderm cell migration. Tracking of mesoderm cell migration in htl^{M+Z-} mutant embryos demonstrated that movement is non-collective and a monolayer is not achieved, but did not identify any cell division phenotype in comparison with wild type (McMahon et al., 2008). In contrast, mesoderm migration in *mys* mutant embryos exhibited normal migration, like wild type, until the last stage, in which they failed to form a monolayer (McMahon et al., 2010). Here, we used this live imaging plus tracking approach to obtain additional insight into phenotypes associated with ectopic expression of the ligand Ths as well as knockdown of Baz, both in a mesoderm-specific manner. These two mutations appear to impact spreading in opposite ways from analysis of fixed samples (e.g. see Fig. 5M-N and Fig. S2M,N).

Initially, in movies of H2A-GFP transgene-containing embryos that also ectopically express Ths ligand through twi_h*-Gal4* (Fig. 7A, B; and Movie 2), we found that cells barely move in the angular direction (Fig. 7C,G, Fig. S3C) compared with the normal spreading behavior exhibited by wild-type mesoderm cells (Fig. 7C,F, Fig. S3B; Movie 1; see also McMahon et al., 2008). A metric of collective cell migration (A) can be used to quantify this behavior that relates the azimuthal angular position of a cell at the beginning of the migration compared with its position at the end of the migration, when movements in the embryos are translated into cylindrical coordinates (Fig. 7A,B, Fig. S3A) (McMahon et al., 2008). When these data are plotted for each cell in the migrating collective, the slope of the line is a measure of the degree of spreading and the coefficient R characterizes the collective nature of cell movements. For wild type, A is close to 2, as also demonstrated previously, whereas upon ectopic expression of Ths, we found that A=1 (Fig. S3E,F, respectively). Together, our data show the cells fail to migrate dorsally but remain as a collective (R=0.93, Fig. S3F) upon ectopic expression of Ths in the mesoderm. These results also help explain how loss-of-function (i.e. htl^{M-Z-}) and gain-of-function (i.e. high level twi_h*>ths*) FGF mutants support similar phenotypes that result in increased AJs, but for different reasons. FGF mutants fail to take down AJs at the early stages (e.g. stage 7), resulting in aberrant migration at later stages (e.g. Fig. 5F), whereas ectopic expression of ligand leads to precocious expression of adhesion molecules (i.e. Mys), which accounts for similarly increased AJ number and cell migration phenotypes (e.g. Fig. 5N).

The tracking analysis also enabled us to examine more carefully the role for FGF in regulating cell divisions. In wild-type embryos, mesoderm cells divide twice with a period of about 60 min between divisions; furthermore, those cells located closer to the ectoderm divide earlier than those located at a distance (Fig. 7D,I,L). Upon ectopic expression of Ths, mesoderm cell division is delayed for most cells as the period between cell divisions increases to 90 min (Fig. 7D,J,M). Surprisingly, a subset of cells also undergoes a third division (Fig. 7M, black outlines).

Development (2018) 145, dev161927. doi:10.1242/dev.161927

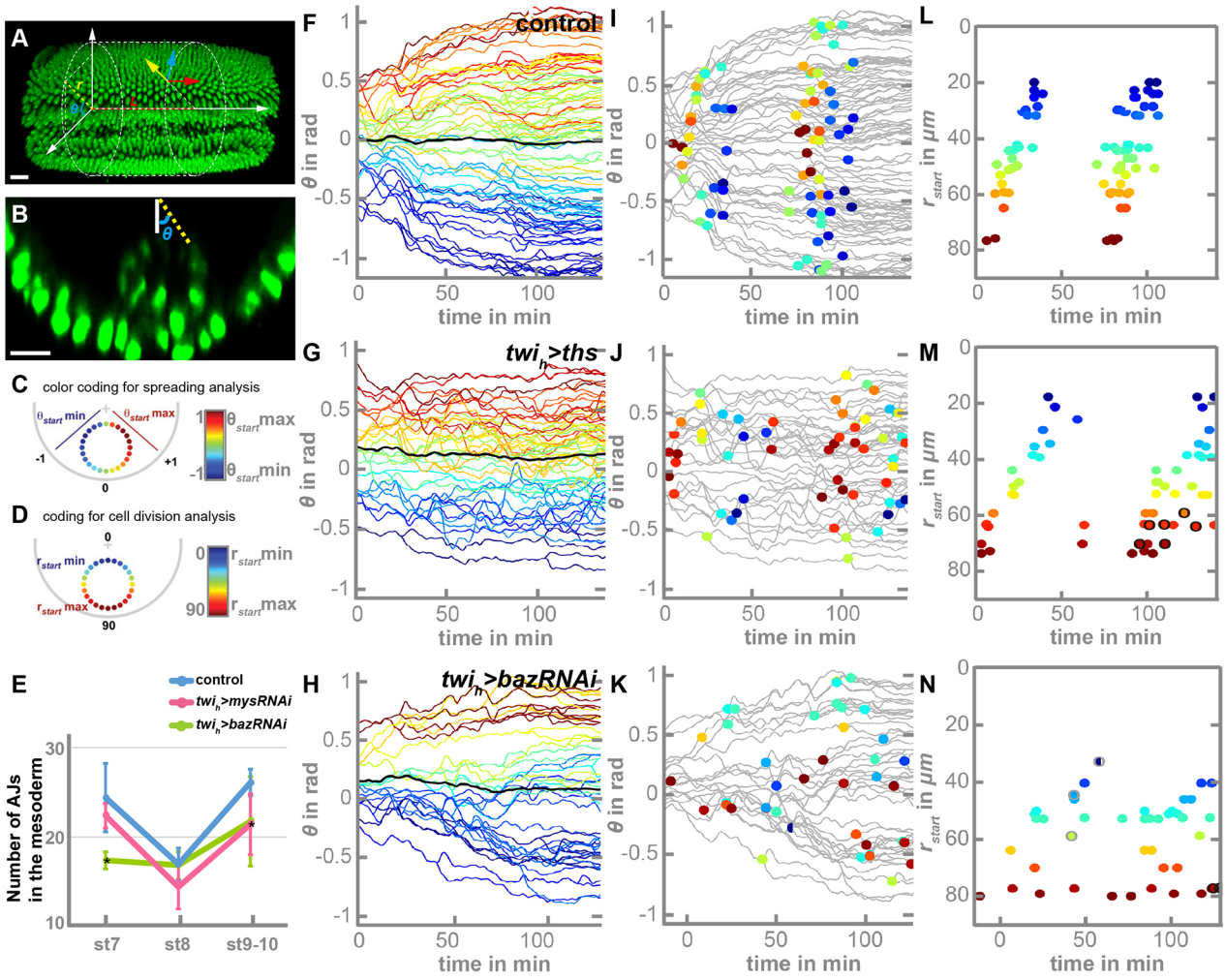

Fig. 7. Live imaging shows that *htl* functions in the mesoderm to control cell division rate and number. (A-D) Tracking of mesoderm cell movement in the embryos was accomplished by following the *in vivo* nuclear signal associated with H2A-GFP transgene in movies obtained by two-photon live imaging (see Materials and Methods and Movies 1-3). (A) Ventral view of embryo showing the fitting of cylindrical coordinates. (B) Posterior view of an embryo showing the invaginated tube and how each single mesoderm cell in the furrow was fitted to cylindrical coordinates. (C) For analysis of cell spreading, cells in the invaginated tube are color-coded based on their azimuthal angular position. (D) For analysis of cell division trends, a color code relating to the radial position of a cell is used (see Materials and Methods). (F,I,L) Tracking analysis from a control embryo (i.e. *yw*) showing movement of mesoderm cells in the angular direction (F) using azimuthal color code (C), position and time of cell divisions superimposed on spreading tracks (I) using radial color code (D), and timing of cell division relative to its radial position (L). The range of azimuthal angular positions of the mesoderm cells changes from –0.5 to 0.5 at the beginning of the migration to –1 to 1 at the end. A measurement of the spreading strength, $A=\theta_{start}/\theta_{end}$ (Fig. S3A,E), has a value close to 2 in the control embryos. In plots I and L, each colored spot represents one cell division. The two mesoderm cell divisions are highly synchronized: cells with bigger *r* value (red, closer to the ectoderm) divide first and cells with smaller *r* value (blue) divide later. (G,J,M) Tracking analysis showing mesoderm spreading phenotypes associated with ectopic expression of Ths ligand (*twi$_h$>ths*) displayed in a similar manner to the control (see F,I,L). Spreading tracks are more confined in G compared with F. Cell divisions are less synchronized in J compared with I. Spots outlined in black in M indicate cells that, unusually, have divided a third time. (H,K,N) Tracking analysis of a *twi$_h$>baz RNAi* embryo of severe phenotype. Some cells cross the midline (black line in the middle, H) and cell divisions are not synchronized (K). (N) Several tracked cells have divided only once in the course of 3 h (outlined in grey), whereas the two cells marked with a black outline have divided a third time. (E) Number of AJs in the mesoderm at stages 7, 8 or 9/10 of indicated genetic backgrounds. Error bars represent s.d. Based on Student *t*-test (*P<0.05), significance was reached in comparison of AJ numbers present in *twi$_h$>mys RNAi* mutants with control at stage 9-10, as well as in *twi$_h$>baz RNAi* mutants at stage 7. Number of embryos for control and mutant background at stages 7, 8 and 9-10 are as follow (total number of *z*-projections counted in the group is indicated in parentheses): control, 5(43), 5(51) and 3(24); *twi$_h$>mys RNAi*, 3(25), 3(24) and 4(35); *twi$_h$>baz RNAi*, 4(39), 6(48) and 5(40). Scale bars: 20 µm.

We also obtained and analyzed movies of H2A-GFP transgenic embryos driving *baz* RNAi in the mesoderm through *twi$_h$-Gal4*. *twi$_h$>baz RNAi* embryos exhibited variations in phenotype, ‘strong’ or ‘weak’, characterized by a delayed invagination or apparently normal invagination, respectively. In addition, the ‘strong’ *baz* RNAi phenotype was associated with non-collective spreading and aberrant cell division (Fig. 7H,K, showing cells cross the midline; R=0.86, data not shown; Movie 3), whereas the ‘weak’ phenotype was associated with decreased spreading strength (A=1.5, Fig. S3G,H; Movie 4) but normal cell division (Fig. S3I,J). Surprisingly, in the embryo exhibiting strong Baz RNAi phenotype, cell division was non-uniform: some cells divide only once (Fig. 7N, gray circles), whereas some divide three times (Fig. 7N, black circles; as observed for *ths* ectopic expression, Fig. 7M). Baz expression was detected throughout the mesoderm-spreading process, and mesoderm-specific *baz* RNAi is associated with a decrease in the number of AJs at both stage 7 and stage 9/10 (Fig. 7E, green line-associated asterisks, P<0.05). Therefore, Baz plays multiple roles in the process of

Development (2018) 145, dev161927. doi:10.1242/dev.161927

mesoderm migration: (1) it maintains or stabilizes AJs facilitating invagination; (2) it ensures a slow decrease in AJ number to support a prolonged EMT and the collectiveness of mesoderm movement; (3) it supports monolayer formation by increasing apical AJ number and reinforcing the basal Mys localization; and (4) it regulates cell division, which may be indirect and dependent on the above functions.

FGF signaling controls EMT by regulating cell division timing and number

Previous studies had suggested that cell divisions contribute to EMT (e.g. Clark et al., 2011). Specifically, in the mesoderm, cells divide at stage 8 as the furrow collapses and mesoderm cells touch down to the ectoderm. Cell division is thought to decrease cell-cell adhesion associated with EMT, possibly by exerting a pulling force between cells as they divide. However, a potential link between mitosis and FGF signaling activity had yet to be investigated. As our tracking analysis had demonstrated that FGF regulates cell division rate, we examined more closely whether FGF mutants exhibit a cell division phenotype at gastrulation.

Using an antibody against phospho-Histone H3 (anti-PH3), it can be observed that mitosis is highly synchronized among the mesoderm cells, as indicated by their uniform staining pattern of PH3: condensed histone staining during tube collapse (Fig. 8A) and histone staining in smaller puncta during segregation and cytokinesis (Fig. 8B) (Shibata et al., 1990; Su et al., 1998). However, this synchrony in cell division is disrupted in the *htl* mutants (Fig. 8H,I,K,L). htl^{M-Z-} embryos exhibit less PH3 staining, suggesting an overall reduced mitotic activity (nine out of nine embryos, Fig. 8K,L); this is supported by the finding that these mutants sometimes contain visibly fewer mesoderm cells (see the gaps in Fig. 3K). In contrast, all cells divide upon high-level ectopic expression of Ths (seven out of seven embryos, Fig. 8E,F), consistent with the tracking analysis, which revealed an additional division in the subset of mesoderm cells in this mutant (Fig. 7J).

How FGF signaling regulates cell division to support EMT is unclear, but it has been noted that the htl^{M+Z-},*stg* double mutant embryo exhibits a prolonged invaginated tube state (Fig. 8Y; Clark et al., 2011). Furthermore, we found that AJs, identified by α- and β-Catenin colocalization, concentrate at the center of the invaginated tube at stage 7, and likely remain in this position until a later stage when the developing midgut primordium becomes prominent (blue arrows, Fig. 8Y compare with W; X, asterisks, $P<0.01$; Fig. S4). Because this blocked-EMT phenotype is much more severe than either *stg* or *htl* single mutant alone, FGF signaling likely also functions through a distinct pathway rather than regulating mitosis to support EMT (Fig. 8D, see Discussion).

To provide insight into its cell division-independent role, we investigated whether FGF signaling impacts the expression of Snail, a well-known transcriptional repressor of E-Cadherin (Cano et al., 2000; Thiery and Sleeman, 2006). However, Snail protein levels in htl^{M+Z-}, htl^{M-Z-} or twi_h>*ths* mutants were largely comparable with those of the control embryo at stage 7 (Fig. 8C,G,J,M), indicating that the differences in the number of AJs observed in FGF loss of function or gain of function mutants (Fig. 2E,F) are not likely due to the lack of Snail.

Most studies in *Drosophila* have focused on how Htl FGFR activation acts through Ras/MAPK; however, FGFRs in other systems can also activate PI3K (Ornitz and Itoh, 2015). We assayed whether Ras- and PI3K-mediated intracellular pathways are responsible for carrying out different parts of the FGF functions during mesoderm development. Surprisingly, we found that $rasC40B^{M-Z-}$ mutant embryos derived from germline clone females (Prober and Edgar, 2000) exhibit spreading defects that may be associated with asynchrony in cell division, in a manner that is similar to what we observed in the *htl* mutants (eight out of eight, Fig. 8K,L,N,O). However, $rasC40B^{M-Z-}$ embryos can form a cell monolayer that acquires apicobasal polarity, as indicated by localization of Baz to the mesoderm-yolk interface (Fig. 8P,P′,R). In contrast, tissue-specific RNAi-mediated knockdown of class III PI3K *Vps34*/PI3K59F (Ribeiro et al., 2011) in the mesoderm has no effect on the timing of cell division (five out of five embryos, Fig. 8S,T), but does result in a dramatic reduction in apical Baz localization (Fig. 8R,U,U′), suggesting a loss of polarity. Together, our data indicate that these two roles of FGF signaling during mesoderm migration are carried out by two different intracellular pathways: a Ras-dependent activity controlling cell division to support spreading/EMT and a PI3K-dependent activity that relates to the reacquisition of cell polarity/MET.

DISCUSSION

Our study demonstrates that FGF signaling serves multiple roles during gastrulation to support this complex morphogenetic process and to direct mesoderm tissue specification. We found that FGF signaling (1) regulates cell division to support EMT, which we show does not only represent the collapse of the tube but continues throughout the mesoderm-spreading process to allow cell movements; (2) establishes cell polarity of the monolayer through control of localization of polarity proteins, including the β-PS integrin Mys to the presumptive basal side of cells; and (3), in a role possibly related to these activities above, regulates AJ number. Modifying FGF levels only led to small changes in cell number through effects on cell division, and the relatively large changes in AJ number could not relate solely to changes in cell number. Therefore, we favor the view that FGF has multiple roles, including regulation of cell division, cell polarity and AJ number. Furthermore, we propose that monolayer formation and re-epithelialization of mesoderm cells through MET is important, because it ensures that subdivision of the mesoderm occurs properly throughout the trunk, allowing accurate specification of different muscle subtypes (Fig. 6).

The role of FGF in supporting EMT is mediated by intracellular Ras signaling, whereas its role in supporting MET requires intracellular PI3K (Fig. 8N-V). The different requirement of intracellular signaling pathway effectors, known to mediate FGF signaling, supports the view that FGF has at least two functions in supporting mesoderm migration and monolayer formation at gastrulation. Furthermore, although activation of Ras has been shown to be an effector of FGF signaling in *Drosophila* (Carmena et al., 1998; e.g. Schulz and Gajewski, 1999), a role for PI3K in supporting FGF-regulated MET is the first characterized activity for this pathway in *Drosophila*, to our knowledge; however, it has been documented in the mammalian system that FGF signaling activates the PI3K pathway (Ornitz and Itoh, 2015). PI3K is also known to directly impact the specification of cell polarity and has been shown to regulate integrin trafficking and cell migration through endocytic pathways (Abe et al., 2009; Ribeiro et al., 2011). Future experiments will aim to define the molecular mechanism by which FGF activation leads to PI3K activation versus Ras; possibly this distinction relates to quality, quantity and direction of input from ligands.

Only a few studies have attempted to link FGF signaling to the establishment of cell polarity, a hallmark component of MET. In *C. elegans* and zebrafish, FGF indirectly regulates cell polarity by

Development (2018) 145, dev161927. doi:10.1242/dev.161927

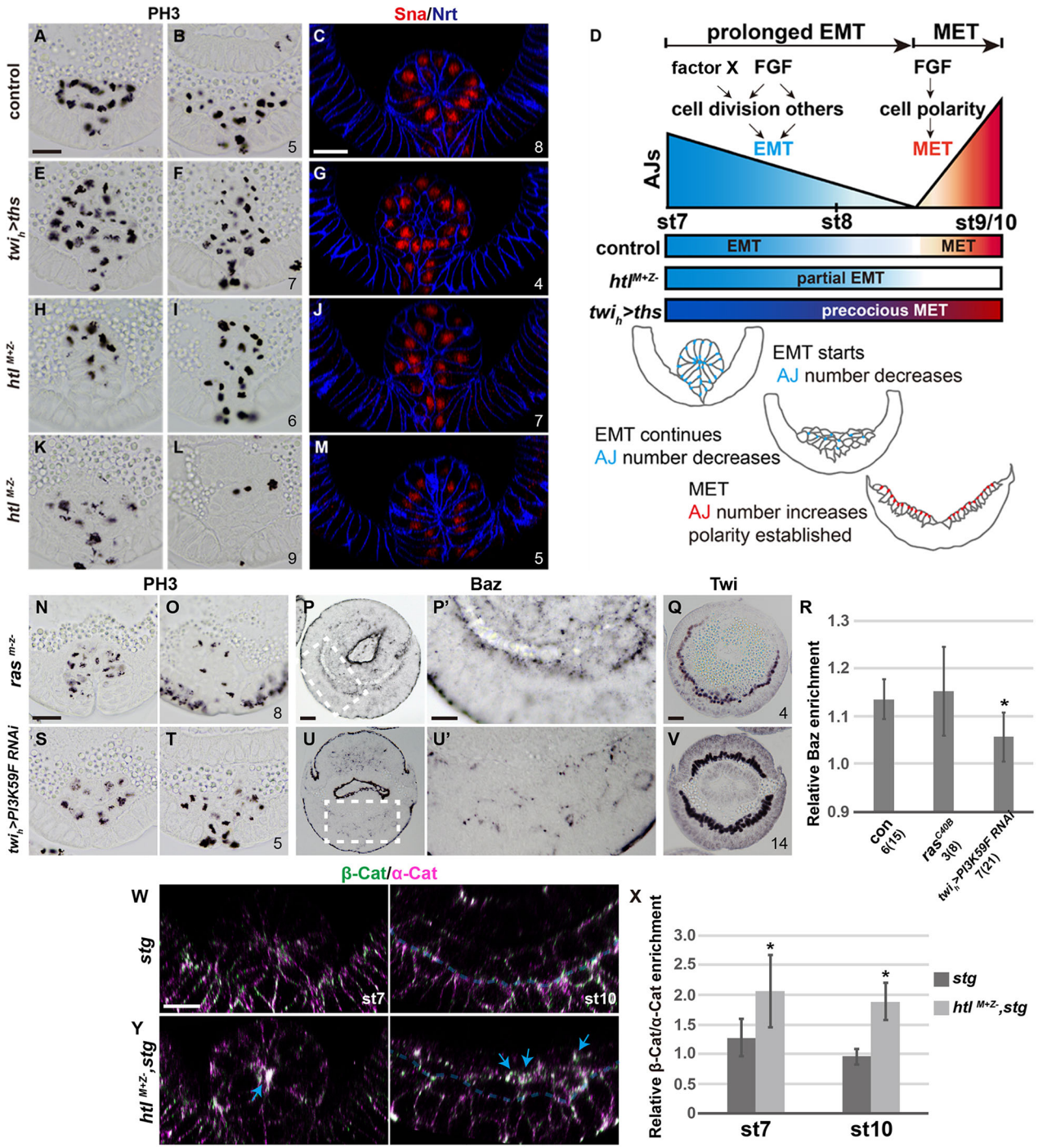

Fig. 8. FGF signaling functions cell-autonomously to drive EMT by regulating cell division and MET by controlling cell polarity. (A,B,E,F,H,I,K,L) Cross-sections of stage 8 embryos stained with anti-phospho-Histone H3 (anti-PH3) antibody to label mitotic cells in embryos of indicated backgrounds (left). (A,E,H,K) The stage of tube collapse, when chromosome condensation is most apparent in the control. (B,F,I,L) Stage of initial spreading, when segregated chromosomes in the daughter cells are also strongly marked by PH3. Number of stage 8 embryos sectioned is indicated in the bottom right-hand corner. (C,G,J,M) *Z*-projections of confocal immunofluorescence scans from stage 7 embryos of indicated genotypes co-stained using anti-Sna (red) and anti-Nrt (blue) antibodies. (D) A model diagram showing how FGF signaling functions to control the EMT and MET of the mesoderm at gastrulation. Blue spots in stage 7 and stage 8 embryos mark the AJs in the mesoderm. Red spots in stage 10 embryo represent AJs that colocalize with Baz. (N-V) Cross-sections of embryos stained with anti-PH3 at stage 8 (N,O,S,T), anti-Baz (P,P′,U,U′) and anti-Twi (Q,V) at stage 10 in ras^{C40B} germline clones and twi_h>*PI3K59F RNAi* mutant backgrounds. Numbers of embryos sectioned are indicated in the bottom right-hand corner in O and T for PH3 and in Q and V for Twi. Boxed regions in P and V are shown at higher magnification in P′ and V′. (R) Quantification of relative Baz enrichment in the mesoderm in P′ and U′ compared with the controls (see Fig. 4A,B). Number of embryos and sections are indicated underneath the genotype (*P<0.005). (W,Y) *Z*-projections from confocal scans of *stg* (W) and htl^{M+Z-},*stg* (Y) embryos co-stained for α-Catenin (violet) and β-Catenin (green) at stages 7 and 10. Strong colocalized signals are observed in between mesoderm cells in htl^{M+Z-},*stg* double mutants (blue arrows, Y). The meso-ectoderm boundary is marked by a semi-transparent blue dashed line at stage 10. (X) Quantification of the relative enrichment of colocalized α- and β-Catenin in the mesoderm in W and Y. Number of embryos (and sections) at stages 7 and 10, respectively, are as follows: *stg*, 3(7) and 3(10); htl^{M+Z},*stg*, 3(6) and 3(10). Significance is reached at both stages when comparing the double mutants with *stg* mutants (*P<0.01). Control refers to a heterozygous zygotic *htl* mutant (i.e. htl^{M+Z-}/+). Scale bars: 20 µm.

Development (2018) 145, dev161927. doi:10.1242/dev.161927

influencing Wnt signaling activity (Minor et al., 2013; Venero Galanternik et al., 2015), whereas in *Ciona intestinalis*, localized signaling by FGF ligands has been shown to directly control asymmetric cell divisions or convergent extension that relies on planar cell polarity components (Cota and Davidson, 2015; Shi et al., 2009). In vertebrates, ectopic activation of FGF signaling has been linked to aberrant growth, resulting in cranial malformation. This suggests that polarized activation of FGF signaling is necessary to provide directional growth (Li et al., 2013). In *Drosophila* embryos, FGF signaling through a different receptor, Breathless, has been shown to regulate E-cadherin turnover to support the collective movement of cells in the gut (Parés and Ricardo, 2015), and mutation in polarity proteins such as Cdc42 results in mesoderm-spreading defects (Clark et al., 2011). Our results have demonstrated a previously uncharacterized role for FGF in supporting mesoderm cell polarity, as well as the importance of the directional activation of the FGF receptor in this context, because HtlCA is not able to rescue the polarity phenotype exhibited by htl^{M+Z-} mutants whereas the wild-type Htl gene can (Fig. 5C,K compared with G,O; Q,R).

We also found that at the end of spreading, E-Cad and N-Cad are both expressed in the mesoderm monolayer, but in a complementary manner: E-Cad is at the basal side, whereas N-Cad is in the apicolateral domain. This complementary expression pattern of cadherins has been observed in other tissues and cell types, such as the dental epithelial cells of fish and mammals (Heymann et al., 2002; Verstraeten et al., 2013) and the ommatidia of the *Drosophila* retina (Chan et al., 2017; Mirkovic and Mlodzik, 2006). In the ommatidia, Wnt and EGF signaling pathways are integrated through E-Cad and N-Cad, which have opposing effects on their rotation through interactions with the cytoskeleton components. The precise cell arrangement and the coordinated cell movement require the cadherins to be expressed in the correct domain at correct level. The fact that mesoderm cells also place E-Cad and N-Cad in complementary cellular domains suggests that AJs at the apical and basal side of the mesoderm are of distinct organization and may carry out different functions, possibly interacting with different signaling pathways, such as Wnt, Dpp and FGF.

The epithelial state of the mesoderm monolayer, achieved at the end of gastrulation, has been previously underappreciated, but our analysis suggests the monolayer is important in integrating different signaling pathways and ensuring the uniform distribution of different precursor lineages derived from mesoderm. At this stage, the combination and level of Dpp, Wnt and FGF signaling received by mesoderm cells will determine what type of muscle the cells will differentiate into. Therefore, forming a monolayer facilitates effective induction of consistent number of precursors from each hemisegment. In addition, the polarized expression of adhesion molecules such as Mys, E-Cad and N-Cad also serve as signal integrators (Moser et al., 2009; Wheelock and Johnson, 2003), making the signal transduction more efficient and regulated.

Alternatively, FGF signaling is generally linked to the regulation of EMT, but this role often involves regulation of Snail expression levels (Ciruna and Rossant, 2001). We found no clear evidence that Snail expression requires FGF, but did uncover that FGF signaling regulates cell division as well as supports another undefined activity that promotes EMT: htl^{M+Z-}*,stg* double mutant phenotypes are more severe than *stg* mutant alone. Like Htl, mutants for the Rho GTP exchange factor Pebble also impact mesoderm cell division and spreading; however, it is thought that Pebble and FGF work in parallel pathways (Gregory et al., 2010). We show that htl^{M-Z-} mutants exhibit decreased proliferation, whereas upon *ths* ligand ectopic expression proliferation is increased (Figs 7M and 8E,F). However, htl^{M+Z-}*,stg* double mutants exhibit stabilized AJs that appear to delay the tube collapse, retaining apical-inside organization at later stage 9/10. In addition, previous studies have shown that cell-cell junctions are mechanosensitive (Weng and Wieschaus, 2016), and therefore future studies should involve deciphering the interplay between FGF signaling, cell division and membrane tension.

We propose that regulation of cell division by FGF may be a conserved mechanism of action in which a slow, prolonged EMT is directed by this pathway in order to support collective cell migration. A gradual decrease in AJs as accomplished by cell division that is controlled by both Stg/Cdc25 and the FGF-Ras pathway may allow the mesoderm cells to maintain just enough cell-cell contacts to ensure that movement as a group is collective (reviewed by Campbell and Casanova, 2016). How migrating cells manage decisions to divide, changes in cell shape (including protrusive activity), acquire cell polarity and initiate differentiation programs remains to be determined, but more-recent studies have shown that sometimes these processes are interdependent (Matus et al., 2015) and this is also likely the case at gastrulation.

MATERIALS AND METHODS

Fly stocks and genetic crosses

All the fly stocks and crosses were maintained at 25°C. *htl-mCherry* was generated through an in-frame insertion of the mCherry reporter into a *htl* construct that is able to rescue the mutant phenotype (Irizarry and Stathopoulos, 2015). *htlAB42/TM3,ftz-lacZ* (#5370), *His2AV-GFP* (#5961), *twi-GAL4* (#914; Carmena et al., 1998; Greig and Akam, 1993; and #58804; Lee et al., 2003; Marqués et al., 2002), *string7M53* (#2500; Jürgens et al., 1984), shg^{GFP} (#60584) *UAS-baz-GFP* (#29037; Benton and St Johnston, 2003), *UASp-baz-mCherry* (#65844; Harris and Peifer, 2005), *UASp-baz-GFP* (#65845; McKinley et al., 2012) and *UAS-mys RNAi* (#33642; Zhai et al., 2012) were obtained from the Bloomington stock center. *UAS-baz RNAi* (GD2914; McDonald et al., 2008) and *UAS-PI3K59F RNAi* (KK100962; Ribeiro et al., 2011) were from the VDRC stock center. *UAS-ths* [AMS289-22] (Stathopoulos et al., 2004), *UAS-pyr* [AMS330-3] (Kadam et al., 2009) and *UAS-htlCA* (Michelson et al., 1998) have been described previously. *FRT101,mysXG43/FM7c,ftz-lacZ* and *UAS-mys,UAs-srcEGFP/CyO,ftz-lacZ* were gifts from Dr Hilary L. Ashe (University of Manchester, UK) (Sawala et al., 2015; Schöck and Perrimon, 2003; Wieschaus et al., 1984). *htlAB42* (Irizarry and Stathopoulos, 2015), *rasC40B* (Prober and Edgar, 2000) and *mysXG43* (Boube et al., 2001; Leptin et al., 1989) germline clones were made using standard FRT-mediated germline clone methodology (Chou and Perrimon, 1996). *htl, stg* double mutants were made through homologous recombination of *htlAB42* and *string7M53*. The *twi-GAL4* driver on the first chromosome (#914) exhibits stronger expression in the embryonic mesoderm and is referred to as twi_h*-GAL4*; the one inserted on the third chromosome (#58804) is referred to as twi_l*-GAL4*. The genotype 'control' in this study refers to *htlAB42/TM3* heterozygote, unless mentioned otherwise.

In situ hybridization, immunohistochemistry, plastic sectioning and immunofluorescence

To examine the transcription level of *bap* and *mys*, antisense RNA probes were labeled with digoxigenin and recognized by anti-DIG antibody conjugated to alkaline phosphatase (1:200, Roche Applied Science). NBT and BCIP were used as substrates for signal detection. Primary antibodies used in this study were: rabbit anti-β-Gal (1:1000, Invitrogen, A-11132), goat anti-GFP (1:5000, Rockland, 600-103-215), rabbit anti-GFP (1:400, Abcam, ab6556), rabbit anti-RFP (1:400, BML PM005), mouse anti-Armadillo (1:40, DSHB, N2 7A1 Armadillo), rat anti-α-Catenin (1:40, DSHB, DCAT-1), rat anti-DE-cadherin (1:40, DSHB, DCAD2), rat anti-Twist (1:200, made in house; Trisnadi and Stathopoulos, 2014), mouse anti-Neurotactin (1:40, DSHB BP 106 anti-Neurotactin), mouse anti-even skipped (1:50, DSHB 2B8), rabbit anti-Htl (1:200, a gift from Dr Alan

Development (2018) 145, dev161927. doi:10.1242/dev.161927

Michelson, Harvard Medical School, USA; Michelson et al., 1998), rabbit anti-Baz (1:500, a gift from Dr Jennifer Zallen, Sloan Kettering Institute, USA; Blankenship et al., 2006), mouse anti-βPS (1:40, DSHB, CF.6G11), rat anti-DN-Cadherin (1:200, DSHB, DN-Ex #8), goat anti-aPKC (1:200, Santa Cruz Biotechnology, C-20), guinea pig anti-Sna (1:1000, a gift from Dr Eric Wieschaus, Princeton University, USA; Weng and Wieschaus, 2016) and rabbit anti-PH3 (1:400, Millipore, 06-570). For chromogenic staining, VECTASTAIN Elite ABC system was used in combination with DAB substrate for signal development (Vector Lab). For immunofluorescence, Alexa Fluor 488, 555 and 647 secondary antibodies were used (Molecular Probes). DAPI (Molecular Probes) was used for counterstaining. Embryos stained with anti-RFP, rabbit anti-GFP, anti-Arm, anti-α-Catenin, anti-Neurotactin, anti-Baz, anti-Sna or rabbit anti-Htl antibodies were fixed using a heat-methanol method. Standard formaldehyde fixation and staining were used for other antibodies. To quantify Baz immunofluorescent staining, embryos were cleared in 70% glycerol overnight and manually cross-sectioned with a razor blade to remove the anterior and posterior regions along the AP axis. The middle regions were then mounted in 70% glycerol and imaged with LSM 800. Quantification was carried out with the 16-color color lookup table function of ImageJ. Embryos were mounted in Permount (Fisher Scientific) for whole-mount studies or embedded in acetone-araldite (Electron Microscopy Sciences) for cross-sectioning. Plastic sections (8 µm) were obtained using a microtome (LKB Bromna 2218 Historange) and mounted in 1:1 acetone: araldite solution. Fluorescent images were obtained with a LSM 800 confocal microscope (Carl Zeiss).

AJ counting and statistics

To compare the adhesion property of the mesoderm cells among the wild type and mutants, we used an anti-α-Catenin and an anti-Armadillo (i.e. β-Catenin) antibody simultaneously to label the AJs, and an anti-Htl antibody to determine the genotype of the embryos. Embryos from stage 7 to 10 were collected from control (htl^{M+Z-}/*TM3*), htl^{M+Z-}, htl^{M-Z+}, htl^{M-Z-}, twi_h>*ths*, twi_h>*htlCA*, twi_h>*mys RNAi* and twi_h>*baz RNAi* mutants, and fixed by heat. Standard immunofluorescence staining procedure was followed and all the stained embryos were manually picked, positioned on the slides that were pre-coated with heptane glue and mounted in 70% glycerol. Confocal scans of 68-100 µm along the *z*-axis were taken with Zeiss LSM 800. For each embryo, 8-10 *z*-projections through the middle one-third along the body axis from its 3D reconstructed image were collected and used to count the AJs. To count the number of AJs in the mesoderm on one *z*-projection, we used Photoshop (Adobe) to mark the boundary between mesoderm and ectoderm, increase the contrast and lower the exposure offset to make the white colocalization signals between α-Catenin (violet) and Armadillo (green) more visible. The microscope settings were kept the same as much as possible, except that more laser power were used in mutant embryos with a taller furrow. All the images were processed the same way. A mean of AJs numbers in the mesoderm was first calculated from all the cross-sections for each embryo. Then, an average (as the mean of the group) and a standard deviation (s.d.) were calculated for the embryos that were pooled together based on their genotypes and developmental stages. Stage 9 and 10 embryos were combined. Error bars represent s.d. Shapiro-Wilk Normality test was used to test for normal distribution of the means within the group. In the cases with fewer than five individuals (n<5) in the group, we performed the test on the AJs number counted from all the images acquired for the embryos in the group. Our data exhibited normal distribution. Student's *t*-test was used for significance analysis. P<0.05 was considered statistically significant. Number of embryos for each genetic background at stages 7, 8 and 9-10 are as follows, respectively: control, 5, 5 and 3; htl^{M+Z-}, 3, 7 and 6; htl^{M-Z-}, 6, 4 and 4; htl^{M-Z+}, 4, 3 and 3; twi_h>*ths*, 1, 4 and 3; twi_h>*htlCA*, 2, 3 and 3; twi_h>*mys RNAi*, 3, 3 and 4; twi_h>*baz RNAi*, 4, 6 and 5.

Quantification on immunohistochemistry and immunofluorescence images

To analyze chromogenic antibody staining of Baz, Mys, aPKC and E-Cad, each genetic background (normally 50-120 embryos at stages 6-10) were embedded for plastic sectioning. Poorly stained embryos, undeveloped embryos or embryos with morphological defects that are clearly not due to the genetic manipulations were excluded from our analysis. Sections mounted unevenly that were difficult to focus on during imaging were excluded. Bright-field images were photographed with a Zeiss Axio Imager under similar settings. A minimum of five embryos or six sections at each stage were imaged so that normality could be tested. In cases where fewer than five embryos were recovered, we were very confident in the consistency of the phenotype. Images were converted to gray scale, reversed and measured in ImageJ. To calculate the relative enrichment, boxes (ROI) of the same size were placed in the mesoderm and the ectoderm, mean gray value in the mesoderm ROI was divided by the mean gray value in the ectoderm ROI, and the quotient was recorded as one data point. First, an average enrichment was calculated for each embryo. Then the averages and the standard deviations (s.d.) were calculated within the same genetic background. Error bars represent s.d. The Shapiro-Wilk Normality test was used to test for normality. Student's *t*-test was used for significance analysis. Fluorescent anti-Nrt images were analyzed by comparing the percentage of polarized mesoderm cells in the control and mutant embryos. Colocalization of α- and β-Catenin in *stg* and htl^{M+Z-},*stg* embryos was also quantified by measuring the mean gray value in the ROI. Similarly, the quotients were compared between the two lines.

Two-photon imaging, cell tracking and analysis

Two twi_h>*ths*, twi_h>*baz RNAi* and *yw* embryos were imaged as previously described using a Zeiss LSM 710 inverted microscope at 940 nm wavelength (McMahon et al., 2008; Supatto et al., 2009). Nuclear tracking was performed using Imaris (Bitplane). Imaris data were then exported to Matlab (The Mathworks) for analysis using custom scripts (Supatto et al., 2009). Briefly, distributions of the ectoderm cells were fitted into a cylinder in order to register the 3D positional tracking data in cylindrical coordinates (r, θ and L), which allows the analysis of cell movement along the corresponding body axis of the embryo (Fig. 7A,B). Two different color codes were applied to show the organization of the mesoderm cells (Fig. 7C,D). In a spreading plot θ (t) (Fig. 7F-H), color code marks the angular position of cells in the furrow at stage 7, in order to better depict their spatial displacement over time. t=*0* ($j0$) represents the onset of germ band elongation. *Start* ($jstart$) is the time when the furrow forms the best cylindrical shape, and *end* ($jend$) is defined as 120 min after *start*. For cell division analysis, cells are color coded for their radial position in the furrow to show the difference in division time according to the distance from the ectoderm (Fig. 7I-N). The spreading profile or the θ_{end} (θ_{start}) plot shows how well the mesoderm spreads as a collective, in which the angular position of each cell at the beginning and the end of the spreading process is fitted into a regression line: $\theta_{end}=A.\theta_{start}+B$. The slope A characterizes the general spreading behavior and should be close to 2 in the wild-type embryos. The coefficient R should be close to 1 when the cells are migrating as a collective.

Acknowledgements

We are grateful to H. Ashe, A. Michelson, E. Wieschaus and J. Zallen for sharing fly stocks and antibodies, and to Z. Ákos, F. Macabenta, A. McMahon, W. Supatto and N. Trisnadi for help with *Drosophila* genetics, sharing preliminary results and antibodies, imaging and tracking, comments on the manuscript, and modifications to scripts as well as helpful discussions.

Competing interests

The authors declare no competing or financial interests.

Author contributions

Conceptualization: J.S., A.S.; Methodology: J.S.; Validation: J.S., A.S.; Formal analysis: J.S., A.S.; Investigation: J.S.; Resources: J.S., A.S.; Data curation: J.S.; Writing - original draft: A.S.; Writing - review & editing: J.S., A.S.; Visualization: J.S.; Supervision: A.S.; Project administration: A.S.; Funding acquisition: A.S.

Funding

This work was funded by the National Institutes of Health grant R35GM118146 to A.S. Deposited in PMC for release after 12 months.

Supplementary information

Supplementary information available online at
http://dev.biologists.org/lookup/doi/10.1242/dev.161927.supplemental

References

Abe, M., Setoguchi, Y., Tanaka, T., Awano, W., Takahashi, K., Ueda, R., Nakamura, A. and Goto, S. (2009). Membrane protein location-dependent regulation by PI3K (III) and rabenosyn-5 in Drosophila wing cells. *PLoS ONE* **4**, e7306.

Bae, Y.-K., Trisnadi, N., Kadam, S. and Stathopoulos, A. (2012). The role of FGF signaling in guiding coordinate movement of cell groups. *Cell Adh. Migr.* **6**, 397-403.

Baum, B. and Georgiou, M. (2011). Dynamics of adherens junctions in epithelial establishment, maintenance, and remodeling. *J. Cell Biol.* **192**, 907-917.

Baum, B., Settleman, J. and Quinlan, M. P. (2008). Transitions between epithelial and mesenchymal states in development and disease. *Semin. Cell Dev. Biol.* **19**, 294-308.

Benton, R. and St Johnston, D. (2003). Drosophila PAR-1 and 14-3-3 inhibit Bazooka/PAR-3 to establish complementary cortical domains in polarized cells. *Cell* **115**, 691-704.

Blankenship, J. T., Backovic, S. T., Sanny, J. S. P., Weitz, O. and Zallen, J. A. (2006). Multicellular rosette formation links planar cell polarity to tissue morphogenesis. *Dev. Cell* **11**, 459-470.

Boube, M., Martin-Bermudo, M. D., Brown, N. H. and Casanova, J. (2001). Specific tracheal migration is mediated by complementary expression of cell surface proteins. *Genes Dev.* **15**, 1554-1562.

Campbell, K. and Casanova, J. (2016). A common framework for EMT and collective cell migration. *Development* **143**, 4291-4300.

Cano, A., Pérez-Moreno, M. A., Rodrigo, I., Locascio, A., Blanco, M. J., del Barrio, M. G., Portillo, F. and Angela Nieto, M. (2000). The transcription factor Snail controls epithelial–mesenchymal transitions by repressing E-cadherin expression. *Nat. Cell Biol.* **2**, 76-83.

Carmena, A., Gisselbrecht, S., Harrison, J., Jiménez, F. and Michelson, A. M. (1998). Combinatorial signaling codes for the progressive determination of cell fates in the Drosophila embryonic mesoderm. *Genes Dev.* **12**, 3910-3922.

Chan, E. H., Chavadimane Shivakumar, P., Clément, R., Laugier, E. and Lenne, P.-F. (2017). Patterned cortical tension mediated by N-cadherin controls cell geometric order in the Drosophila eye. *eLife* **6**, e27796

Chou, T. B. and Perrimon, N. (1996). The autosomal FLP-DFS technique for generating germline mosaics in Drosophila melanogaster. *Genetics* **144**, 1673-1679.

Ciruna, B. and Rossant, J. (2001). FGF signaling regulates mesoderm cell fate specification and morphogenetic movement at the primitive streak. *Dev. Cell* **1**, 37-49.

Clark, I. B. N., Muha, V., Klingseisen, A., Leptin, M. and Müller, H.-A. J. (2011). Fibroblast growth factor signalling controls successive cell behaviours during mesoderm layer formation in Drosophila. *Development* **138**, 2705-2715.

Clarkson, M. and Saint, R. (1999). A His2AvDGFP fusion gene complements a lethal His2AvD mutant allele and provides an in vivo marker for Drosophila chromosome behavior. *DNA Cell Biol.* **18**, 457-462.

Cota, C. D. and Davidson, B. (2015). Mitotic membrane turnover coordinates differential induction of the heart progenitor lineage. *Dev. Cell* **34**, 505-519.

Edgar, B. A. and O'Farrell, P. H. (1989). Genetic control of cell division patterns in the Drosophila embryo. *Cell* **57**, 177-187.

Fernandes, V. M., McCormack, K., Lewellyn, L. and Verheyen, E. M. (2014). Integrins regulate apical constriction via microtubule stabilization in the Drosophila eye disc epithelium. *Cell Rep.* **9**, 2043-2055.

Fernández-Miñán, A., Cobreros, L., González-Reyes, A. and Martín-Bermudo, M. D. (2008). Integrins contribute to the establishment and maintenance of cell polarity in the follicular epithelium of the Drosophila ovary. *Int. J. Dev. Biol.* **52**, 925-932.

Frasch, M. (1995). Induction of visceral and cardiac mesoderm by ectodermal Dpp in the early Drosophila embryo. *Nature* **374**, 464-467.

Frasch, M., Hoey, T., Rushlow, C., Doyle, H. and Levine, M. (1987). Characterization and localization of the even-skipped protein of Drosophila. *EMBO J.* **6**, 749-759.

Gilmour, D., Rembold, M. and Leptin, M. (2017). From morphogen to morphogenesis and back. *Nature* **541**, 311-320.

Gisselbrecht, S., Skeath, J. B., Doe, C. Q. and Michelson, A. M. (1996). heartless encodes a fibroblast growth factor receptor (DFR1/DFGF-R2) involved in the directional migration of early mesodermal cells in the Drosophila embryo. *Genes Dev.* **10**, 3003-3017.

Gregory, S. L., Lorensuhewa, N. and Saint, R. (2010). Signalling through the RhoGEF Pebble in Drosophila. *IUBMB Life* **62**, 290-295.

Greig, S. and Akam, M. (1993). Homeotic genes autonomously specify one aspect of pattern in the Drosophila mesoderm. *Nature* **362**, 630-632.

Gryzik, T. and Müller, H.-A. J. (2004). FGF8-like1 and FGF8-like2 encode putative ligands of the FGF receptor Htl and are required for mesoderm migration in the Drosophila gastrula. *Curr. Biol.* **14**, 659-667.

Harris, T. J. C. and Peifer, M. (2004). Adherens junction-dependent and -independent steps in the establishment of epithelial cell polarity in Drosophila. *J. Cell Biol.* **167**, 135-147.

Harris, T. J. C. and Peifer, M. (2005). The positioning and segregation of apical cues during epithelial polarity establishment in Drosophila. *J. Cell Biol.* **170**, 813-823.

Heymann, R., About, I., Lendahl, U., Franquin, J.-C., Öbrink, B. and Mitsiadis, T. A. (2002). E- and N-cadherin distribution in developing and functional human teeth under normal and pathological conditions. *Am. J. Pathol.* **160**, 2123-2133.

Irizarry, J. and Stathopoulos, A. (2015). FGF signaling supports Drosophila fertility by regulating development of ovarian muscle tissues. *Dev. Biol.* **404**, 1-13.

Iwai, Y., Usui, T., Hirano, S., Steward, R., Takeichi, M. and Uemura, T. (1997). Axon patterning requires DN-cadherin, a novel neuronal adhesion receptor, in the Drosophila embryonic CNS. *Neuron* **19**, 77-89.

Jürgens, G., Wieschaus, E., Nüsslein-Volhard, C. and Kluding, H. (1984). Mutations affecting the pattern of the larval cuticle in Drosophila melanogaster: II. Zygotic loci on the third chromosome. *Wilehm Roux Arch. Dev. Biol.* **193**, 283-295.

Kadam, S., McMahon, A., Tzou, P. and Stathopoulos, A. (2009). FGF ligands in Drosophila have distinct activities required to support cell migration and differentiation. *Development* **136**, 739-747.

Kolsch, V., Seher, T., Fernandez-Ballester, G. J., Serrano, L. and Leptin, M. (2007). Control of Drosophila gastrulation by apical localization of adherens junctions and RhoGEF2. *Science* **315**, 384-386.

Laprise, P. and Tepass, U. (2011). Novel insights into epithelial polarity proteins in Drosophila. *Trends Cell Biol.* **21**, 401-408.

Lee, H.-H., Norris, A., Weiss, J. B. and Frasch, M. (2003). Jelly belly protein activates the receptor tyrosine kinase Alk to specify visceral muscle pioneers. *Nature* **425**, 507-512.

Leptin, M. and Grunewald, B. (1990). Cell shape changes during gastrulation in Drosophila. *Development* **110**, 73-84.

Leptin, M., Bogaert, T., Lehmann, R. and Wilcox, M. (1989). The function of PS integrins during Drosophila embryogenesis. *Cell* **56**, 401-408.

Li, X., Young, N. M., Tropp, S., Hu, D., Xu, Y., Hallgrímsson, B. and Marcucio, R. S. (2013). Quantification of shape and cell polarity reveals a novel mechanism underlying malformations resulting from related FGF mutations during facial morphogenesis. *Hum. Mol. Genet.* **22**, 5160-5172.

MacKrell, A. J., Blumberg, B., Haynes, S. R. and Fessler, J. H. (1988). The lethal myospheroid gene of Drosophila encodes a membrane protein homologous to vertebrate integrin beta subunits. *Proc. Natl. Acad. Sci. USA* **85**, 2633-2637.

Marqués, G., Bao, H., Haerry, T. E., Shimell, M. J., Duchek, P., Zhang, B. and O'Connor, M. B. (2002). The Drosophila BMP type II receptor Wishful Thinking regulates neuromuscular synapse morphology and function. *Neuron* **33**, 529-543.

Matus, D. Q., Lohmer, L. L., Kelley, L. C., Schindler, A. J., Kohrman, A. Q., Barkoulas, M., Zhang, W., Chi, Q. and Sherwood, D. R. (2015). Invasive cell fate requires G1 cell-cycle arrest and histone deacetylase-mediated changes in gene expression. *Dev. Cell* **35**, 162-174.

McDonald, J. A., Khodyakova, A., Aranjuez, G., Dudley, C. and Montell, D. J. (2008). PAR-1 kinase regulates epithelial detachment and directional protrusion of migrating border cells. *Curr. Biol.* **18**, 1659-1667.

McKinley, R. F. A., Yu, C. G. and Harris, T. J. C. (2012). Assembly of Bazooka polarity landmarks through a multifaceted membrane-association mechanism. *J. Cell Sci.* **125**, 1177-1190.

McMahon, A., Supatto, W., Fraser, S. E. and Stathopoulos, A. (2008). Dynamic analyses of Drosophila gastrulation provide insights into collective cell migration. *Science* **322**, 1546-1550.

McMahon, A., Reeves, G. T., Supatto, W. and Stathopoulos, A. (2010). Mesoderm migration in Drosophila is a multi-step process requiring FGF signaling and integrin activity. *Development* **137**, 2167-2175.

Michelson, A. M., Gisselbrecht, S., Zhou, Y., Baek, K.-H. and Buff, E. M. (1998). Dual functions of the heartless fibroblast growth factor receptor in development of the Drosophila embryonic mesoderm. *Dev. Genet.* **22**, 212-229.

Minor, P. J., He, T.-F., Sohn, C. H., Asthagiri, A. R. and Sternberg, P. W. (2013). FGF signaling regulates Wnt ligand expression to control vulval cell lineage polarity in C. elegans. *Development* **140**, 3882-3891.

Mirkovic, I. and Mlodzik, M. (2006). Cooperative activities of drosophila DE-cadherin and DN-cadherin regulate the cell motility process of ommatidial rotation. *Development* **133**, 3283-3293.

Moser, M., Legate, K. R., Zent, R. and Fässler, R. (2009). The tail of integrins, talin, and kindlins. *Science* **324**, 895-899.

Muha, V. and Müller, H.-A. J. (2013). Functions and mechanisms of Fibroblast Growth Factor (FGF) signalling in Drosophila melanogaster. *Int. J. Mol. Sci.* **14**, 5920-5937.

Müller, H. A. and Wieschaus, E. (1996). armadillo, bazooka, and stardust are critical for early stages in formation of the zonula adherens and maintenance of the polarized blastoderm epithelium in Drosophila. *J. Cell Biol.* **134**, 149-163.

Murray, M. J. and Saint, R. (2007). Photoactivatable GFP resolves Drosophila mesoderm migration behaviour. *Development* **134**, 3975-3983.

Narasimha, M. and Brown, N. H. (2013). *Integrins and Associated Proteins in Drosophila Development*. Austin, TX: Landes Bioscience.

Nieto, M. A. (2013). Epithelial plasticity: a common theme in embryonic and cancer cells. *Science* **342**, 1234850.

Oda, H., Uemura, T., Harada, Y., Iwai, Y. and Takeichi, M. (1994). A Drosophila homolog of cadherin associated with armadillo and essential for embryonic cell-cell adhesion. *Dev. Biol.* **165**, 716-726.
Oda, H., Tsukita, S. and Takeichi, M. (1998). Dynamic behavior of the cadherin-based cell-cell adhesion system during Drosophila gastrulation. *Dev. Biol.* **203**, 435-450.
Ornitz, D. M. and Itoh, N. (2015). The Fibroblast Growth Factor signaling pathway. *Wiley Interdiscip. Rev. Dev. Biol.* **4**, 215-266.
Parés, G. and Ricardo, S. (2015). FGF control of E-cadherin targeting in the Drosophila midgut impacts on primordial germ cell motility. *J. Cell Sci.* **129**, 354-366.
Prober, D. A. and Edgar, B. A. (2000). Ras1 promotes cellular growth in the Drosophila wing. *Cell* **100**, 435-446.
Ribeiro, I., Yuan, L., Tanentzapf, G., Dowling, J. J. and Kiger, A. (2011). Phosphoinositide regulation of integrin trafficking required for muscle attachment and maintenance. *PLoS Genet.* **7**, e1001295.
Roegiers, F., Younger-Shepherd, S., Jan, L. Y. and Jan, Y. N. (2001). Bazooka is required for localization of determinants and controlling proliferation in the sensory organ precursor cell lineage in Drosophila. *Proc. Natl. Acad. Sci. USA* **98**, 14469-14474.
Roote, C. E. and Zusman, S. (1995). Functions for PS integrins in tissue adhesion, migration, and shape changes during early embryonic development in Drosophila. *Dev. Biol.* **169**, 322-336.
Sawala, A., Scarcia, M., Sutcliffe, C., Wilcockson, S. G. and Ashe, H. L. (2015). Peak BMP responses in the Drosophila embryo are dependent on the activation of integrin signaling. *Cell Rep.* **13**, 1519-1520.
Schafer, G., Narasimha, M., Vogelsang, E. and Leptin, M. (2014). Cadherin switching during the formation and differentiation of the Drosophila mesoderm - implications for epithelial-to-mesenchymal transitions. *J. Cell Sci.* **127**, 1511-1522.
Schöck, F. and Perrimon, N. (2003). Retraction of the Drosophila germ band requires cell-matrix interaction. *Genes Dev.* **17**, 597-602.
Schulz, R. A. and Gajewski, K. (1999). Ventral neuroblasts and the heartless FGF receptor are required for muscle founder cell specification in Drosophila. *Oncogene* **18**, 6818-6823.
Shi, W., Peyrot, S. M., Munro, E. and Levine, M. (2009). FGF3 in the floor plate directs notochord convergent extension in the Ciona tadpole. *Development* **136**, 23-28.
Shibata, K., Inagaki, M. and Ajiro, K. (1990). Mitosis-specific histone H3 phosphorylation in vitro in nucleosome structures. *Eur. J. Biochem.* **192**, 87-93.
Staehling-Hampton, K., Hoffmann, F. M., Baylies, M. K., Rushtont, E. and Bate, M. (1994). dpp induces mesodermal gene expression in Drosophila. *Nature* **372**, 783-786.
Stathopoulos, A., Tam, B., Ronshaugen, M., Frasch, M. and Levine, M. (2004). pyramus and thisbe: FGF genes that pattern the mesoderm of Drosophila embryos. *Genes Dev.* **18**, 687-699.
Su, T. T., Sprenger, F., DiGregorio, P. J., Campbell, S. D. and O'Farrell, P. H. (1998). Exit from mitosis in Drosophila syncytial embryos requires proteolysis and cyclin degradation, and is associated with localized dephosphorylation. *Genes Dev.* **12**, 1495-1503.
Supatto, W., McMahon, A., Fraser, S. E. and Stathopoulos, A. (2009). Quantitative imaging of collective cell migration during Drosophila gastrulation: multiphoton microscopy and computational analysis. *Nat. Protoc.* **4**, 1397-1412.
Tepass, U. and Hartenstein, V. (1994). The development of cellular junctions in the Drosophila embryo. *Dev. Biol.* **161**, 563-596.
Tepass, U., Tanentzapf, G., Ward, R. and Fehon, R. (2001). Epithelial cell polarity and cell junctions in Drosophila. *Annu. Rev. Genet.* **35**, 747-784.
Thiery, J. P. and Sleeman, J. P. (2006). Complex networks orchestrate epithelial–mesenchymal transitions. *Nat. Rev. Mol. Cell Biol.* **7**, 131-142.
Thiery, J. P., Acloque, H., Huang, R. Y. J. and Angela Nieto, M. (2009). Epithelial-mesenchymal transitions in development and disease. *Cell* **139**, 871-890.
Trisnadi, N. and Stathopoulos, A. (2014). Ectopic expression screen identifies genes affecting Drosophila mesoderm development including the HSPG Trol. *G3* **5**, 301-313.
Venero Galanternik, M., Kramer, K. L. and Piotrowski, T. (2015). Heparan sulfate proteoglycans regulate Fgf signaling and cell polarity during collective cell migration. *Cell Rep.* **10**, 414-428.
Verstraeten, B., van Hengel, J., Sanders, E., Van Roy, F. and Huysseune, A. (2013). N-cadherin is required for cytodifferentiation during zebrafish odontogenesis. *J. Dent. Res.* **92**, 365-370.
Weng, M. and Wieschaus, E. (2016). Myosin-dependent remodeling of adherens junctions protects junctions from Snail-dependent disassembly. *J. Cell Biol.* **212**, 219-229.
Weng, M. and Wieschaus, E. (2017). Polarity protein Par3/Bazooka follows myosin-dependent junction repositioning. *Dev. Biol.* **422**, 125-134.
Wheelock, M. J. and Johnson, K. R. (2003). Cadherin-mediated cellular signaling. *Curr. Opin. Cell Biol.* **15**, 509-514.
Wieschaus, E., Nüsslein-Volhard, C. and Jürgens, G. (1984). Mutations affecting the pattern of the larval cuticle in Drosophila melanogaster: III. Zygotic loci on the X-chromosome and fourth chromosome. *Wilehm Roux Arch. Dev. Biol.* **193**, 296-307.
Wilson, R., Vogelsang, E. and Leptin, M. (2005). FGF signalling and the mechanism of mesoderm spreading in Drosophila embryos. *Development* **132**, 491-501.
Wodarz, A., Ramrath, A., Grimm, A. and Knust, E. (2000). Drosophila atypical protein kinase C associates with Bazooka and controls polarity of epithelia and neuroblasts. *J. Cell Biol.* **150**, 1361-1374.
Zhai, Z., Ha, N., Papagiannouli, F., Hamacher-Brady, A., Brady, N., Sorge, S., Bezdan, D. and Lohmann, I. (2012). Antagonistic regulation of apoptosis and differentiation by the Cut transcription factor represents a tumor-suppressing mechanism in Drosophila. *PLoS Genet.* **8**, e1002582.

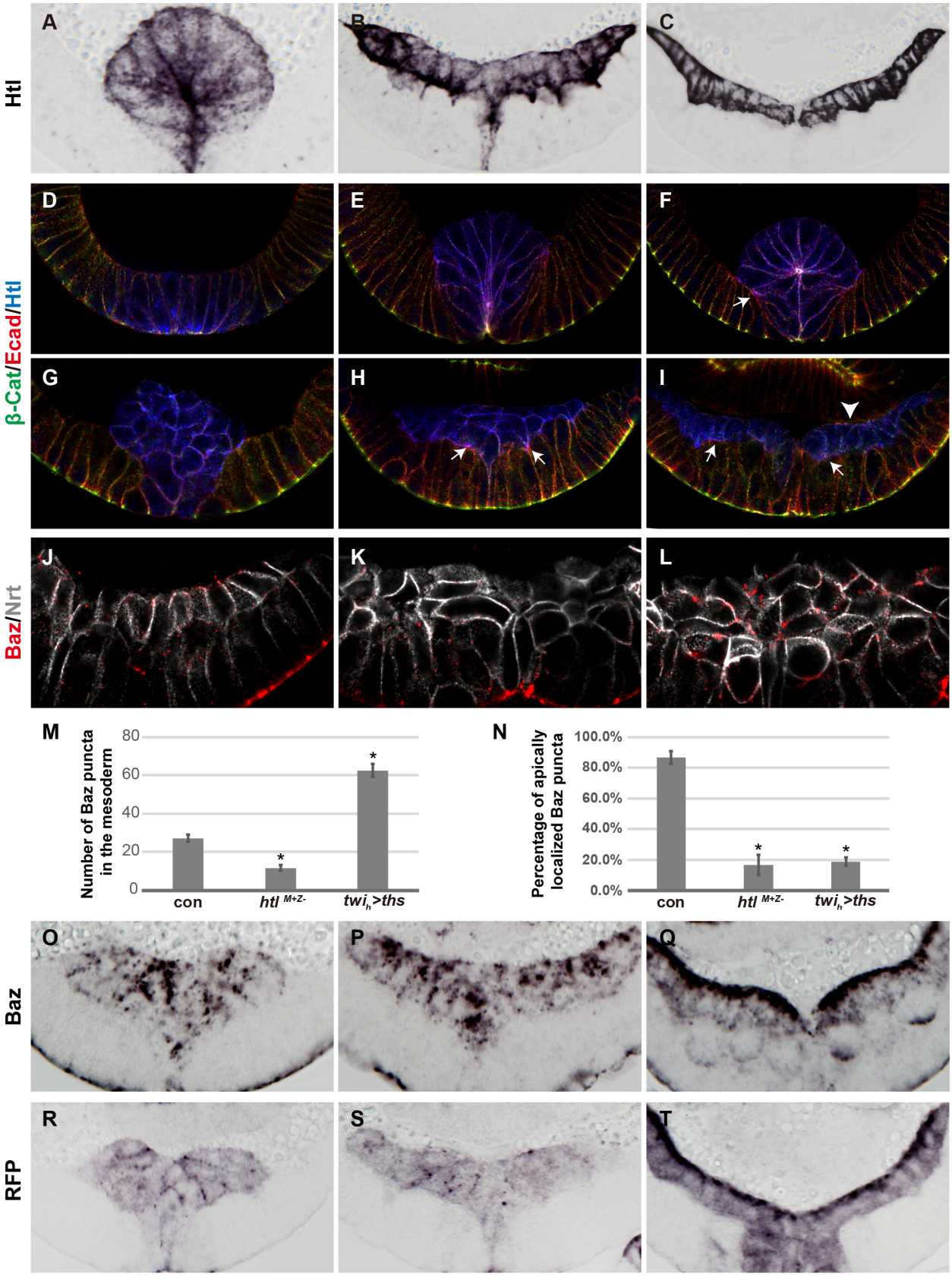

Supplementary Figure 1. Localization of Htl, AJ protein E-Cad, β-Cat and fluorescent protein-tagged Baz with alternative antibodies.

(A-C) Immunostaining of embryos carrying a *htl-mcherry* transgene at stage 7 (A), stage 9 (B), or stage 10 (C) using an anti-RFP antibody.

(D-I) Colocalization using anti-β-Cat (green), anti-E-Cad (red) and anti-Htl (blue) in embryos of stage 6 (D), stage 7 early (E), stage 7 late (F), stage 8 early (G), stage 8 late, and stage 9 (I).

(J-L) Baz (red) fluorescent immunostaining in stage 10 control (J), *htl* $^{M+Z-}$ (K) and *twi$_h$-pyr* (L) embryos. Embryos were co-stained with Nrt (light grey) to visualize the cellular morphology. Confocal single scans shown were taken from manually cross-sectioned embryos.

(M-N) Quantification of Baz expression in J-L. Total number of Baz puncta in the mesoderm is significantly decreased in *htl* $^{M+Z-}$ mutants, but increased in *twi$_h$>ths* embryos compared to the control (asterisks, M, $p<0.001$). Percentage of apically localized Baz puncta is decreased in both mutants (asterisks, N, $p<0.001$). Numbers of embryos for each genetic background at stage 10 are as following (total number of the confocal scans is indicated inside the parenthesis): control: 3(5); *htl*$^{M+Z-}$: 3(3); *twi$_h$>ths*: 7(7). Confocal scans were taken under the same setting. Baz puncta were counted with the same threshold in Image J. Student *t*-test was used to test significance. Error bars represent s.d.

(O-Q) Immunostaining of embryos expressing *baz-GFP* driven by *twi$_h$-GAL4* with anti-Baz antibody at stage 8 early (O), stage 8 late (P), and stage 10 (Q).

(R-T) Immunostaining of embryos expressing *baz-RFP* by the same driver, with anti-RFP antibody at stage 8 early (R), stage 8 late (S), and stage 9/10 (T).

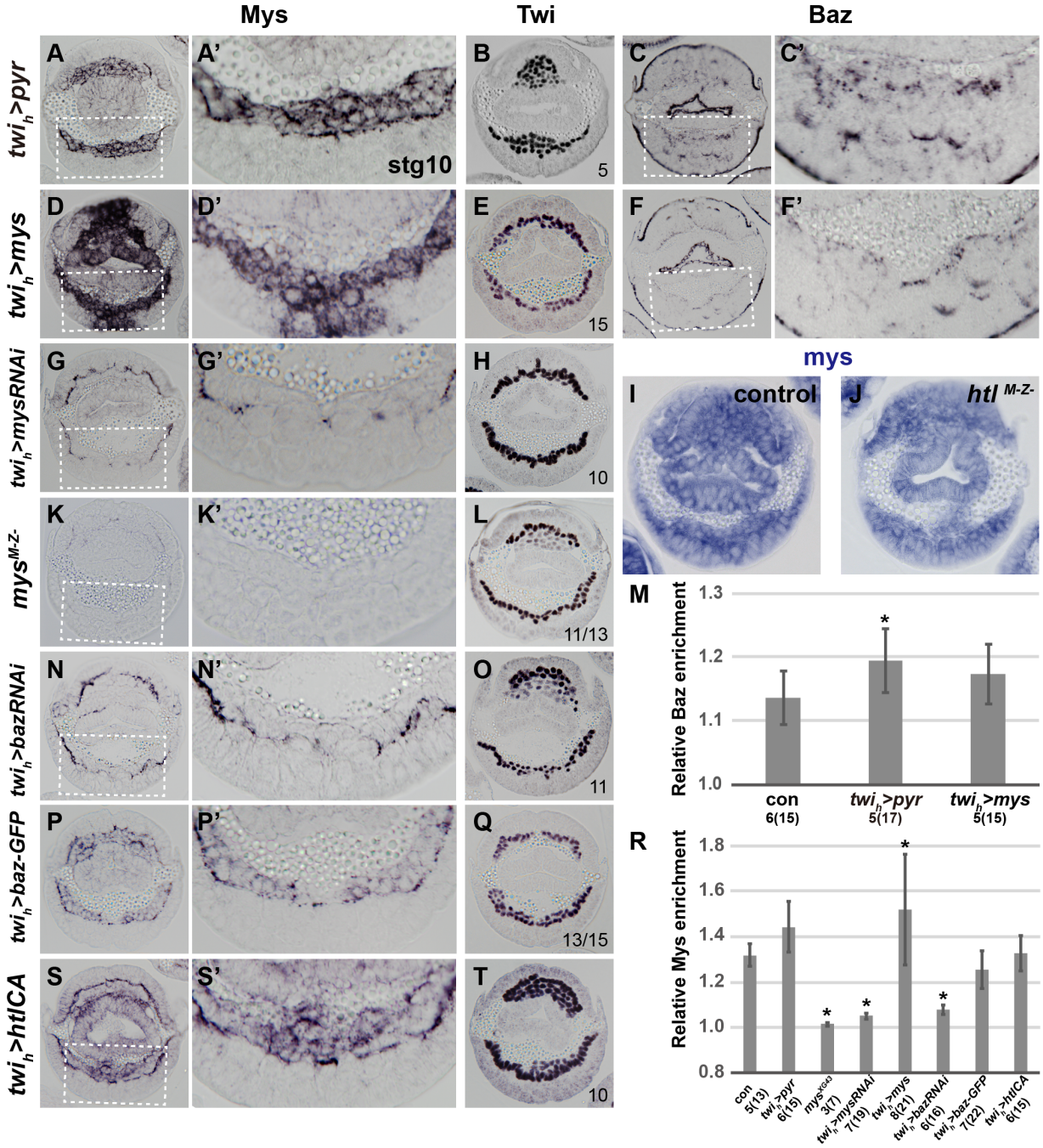

Supplementary Figure 2. Mys and Baz levels in the mesoderm are regulated by FGF. **(A-H,K,L,N-Q,S,T)** Stage 10 embryos of the indicated genotypes immunostained using antibodies against Mys (A,D,G,K,N,P,S and magnified views of boxed regions in A',D',G',K',N',P',S'), Twi (B,E,H,L,O,Q,T) or Baz (C,F and magnified views of boxed regions in C',F'). Number of st10 embryos analyzed by Twi antibody staining is indicated at the bottom right corner in B, E, H, L, O, Q and T. Ratios, if given, represent percentage showing phenotype.

(I, J) Expression of *mys* transcripts detected by in situ hybridization using a riboprobe in control and htl^{M-Z-} mutant embryos around stage 9. *mys* expression is identified in the ectoderm, mesoderm as well as endoderm.
(M) Quantification of relative Baz enrichment in the mesoderm in C' and F' compared to the control (see Fig 4A,B).
(R) Quantification of relative Mys enrichment in the mesoderm-ectoderm interface in A', D', G', K', N', P', S' compared to the control (see Fig 5A',Q).
Number of embryos used for statistical analysis is indicated underneath the genotype with the number of sections inside the parenthesis. Error bars represent s.d. Asterisks represent datapoints that are significantly different from the control based on student *t*-test ($p<0.05$).

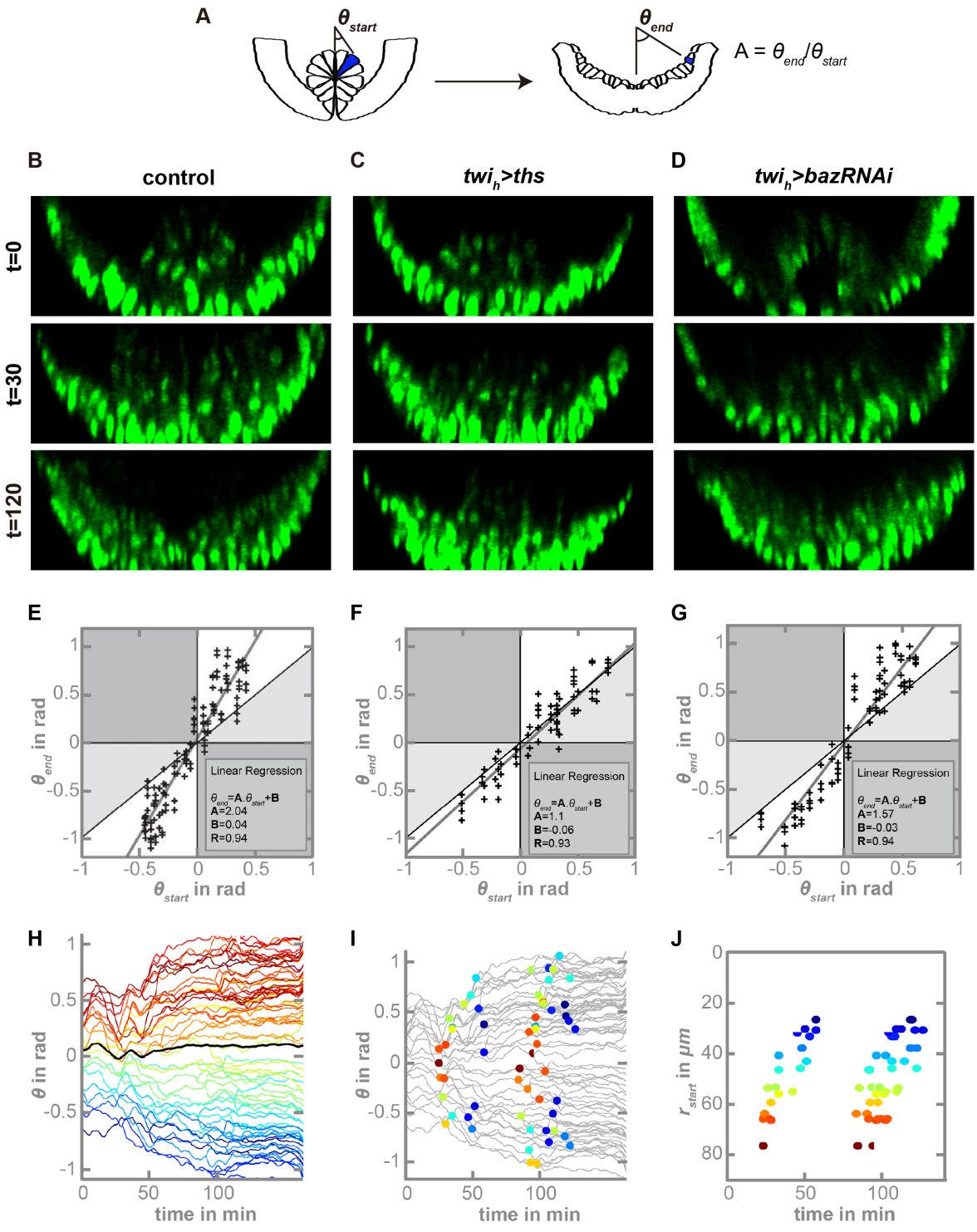

Supplementary Figure 3. Calculation of the mesoderm spreading profile in control, *twi$_h$>ths* and *twi$_h$>baz RNAi* mutant embryos.

(A) Schematic showing how azimuthal angular position changes upon normal spreading movement of cells.

(B-D) Representative stills at the indicated times from movies of embryos of control (B: twi-Gal4 x *yw*), ectopically expressing Ths ligand in the mesoderm (C: twi_h-Gal4 x UAS.ths) and knocking down *baz* in the mesoderm (D: twi_h-Gal4 x UAS.*baz*.RNAi) that also contain the H2A-GFP transgene, which allows visualization of mesoderm cells throughout the course of their migration by live in vivo imaging.
(E-G) Plots of azimuthal angular position, θ_{start} *vs.* θ_{end}, for tracked mesoderm cells in (B), (C) and (D). In control embryo, the slope of the line, A, is close to 2 and has been previously used to define the degree of collective movement of mesoderm cells (McMahon et al., 2008). Upon ectopic expression of Ths, A is reduced to 1 (F), demonstrating that cells do not spread as θ_{start} is equivalent to θ_{end}. In a less severe *twi_h>baz RNAi* embryo that has been tracked (G), A falls between 1 and 2 (θ_{end} is less than twice θ_{start}, as found in the control), suggesting spreading is compromised without Baz participation.
(H-J) See supplemental movie 4. Tracking analysis of the *twi_h>baz RNAi* embryo with a mild spreading phenotype (D,G) displayed in a similar manner to the control (Figure 7F,I,L).

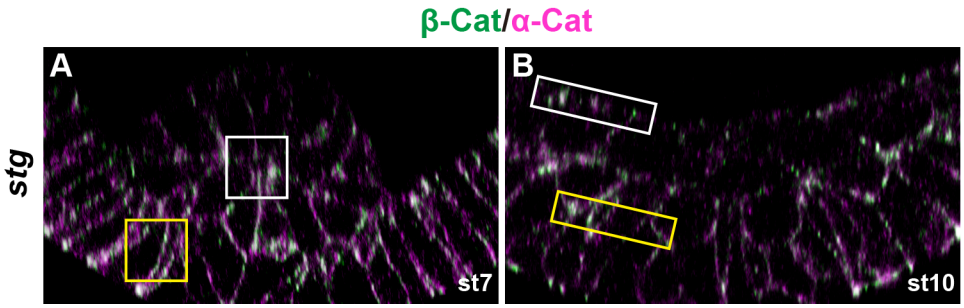

Supplementary Figure 4. Example of calculating the enrichment of colocalized α-Catenin and β-Catenin in the mesoderm. Z-projections from confocal scans of *stg* embryos co-stained by antibodies against α-Catenin (violet) and β-Catenin (green) at stage7 (A) and stage10 (B). Boxes in white indicate the mesoderm signal while boxes in yellow of the same size indicate the ectoderm signal. Gray value measurements were taken for both in Image J. The relative enrichment was calculated by dividing the value in white box by the value in yellow box.

SUPPLEMENTAL MOVIES

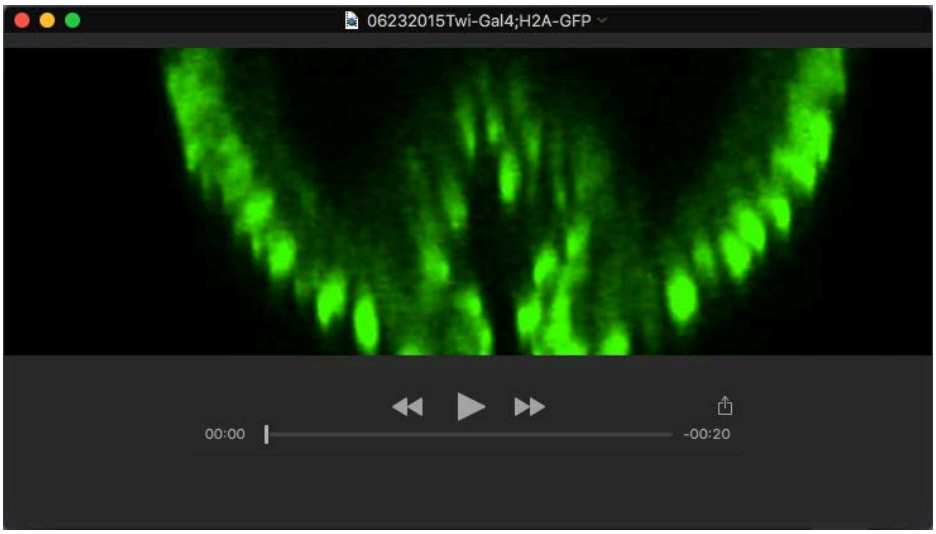

Movie 1 shows mesoderm cell spreading in an embryo containing an H2A-GFP transgene that allows tracking of cell movement in *yw* background.

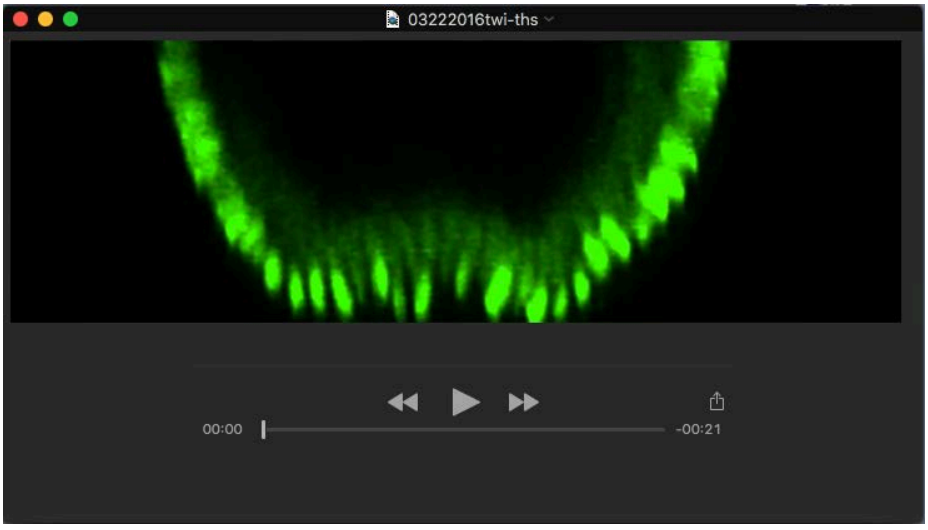

Movie 2 shows mesoderm cell spreading in a *twi$_h$>ths* mutant embryo containing the H2A-GFP transgene.

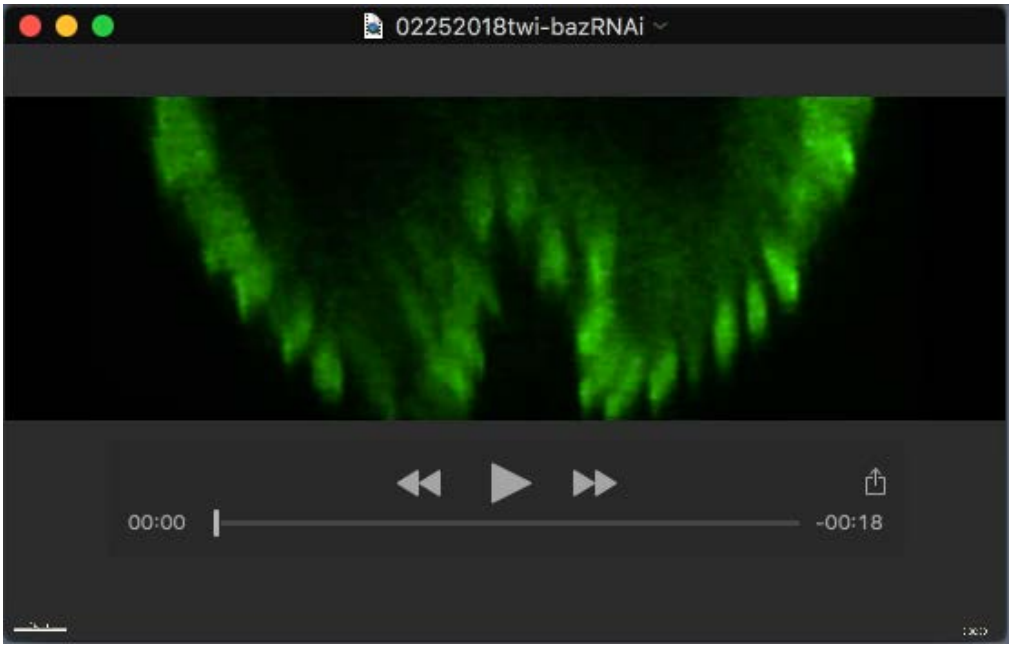

Movie 3 shows mesoderm cell spreading in *twi$_h$>baz RNAi* mutant background, carrying H2A-GFP transgene, that exhibits defects as early as invagination (likely "strong" phenotype)..

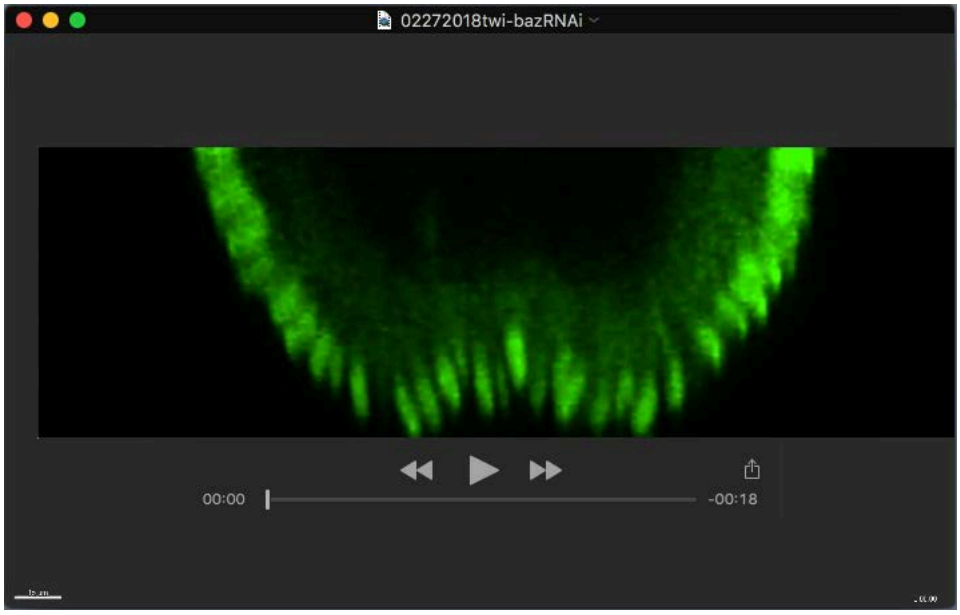

Movie 4 shows mesoderm cell spreading in an H2A-GFP transgenic embryo in *twi$_h$>baz RNAi* mutant background that exhibits normal invagination but mild spreading defect later (likely "mild" phenotype).